

UNIVERSITY OF CRETE
CHEMISTRY DEPARTMENT
POSTGRADUATE PROGRAM ON APPLIED MOLECULAR
SPECTROSCOPY



MICELLIZATION IN
COPOLYMER/HOMOPOLYMER BLENDS.
EFFECT OF ARCHITECTURE AND COMPOSITION

KONSTANTINA KARAGIANNI



FOUNDATION FOR RESEARCH AND TECHNOLOGY-HELLAS
INSTITUTE OF ELECTRONIC STRUCTURE AND LASER

HERAKLION, NOVEMBER 2005

ΠΑΝΕΠΙΣΤΗΜΙΟ ΚΡΗΤΗΣ
ΤΜΗΜΑ ΧΗΜΕΙΑΣ
ΜΕΤΑΠΤΥΧΙΑΚΟ ΠΡΟΓΡΑΜΜΑ ΕΦΗΡΜΟΣΜΕΝΗΣ
ΜΟΡΙΑΚΗΣ ΦΑΣΜΑΤΟΣΚΟΠΟΙΑΣ



ΜΙΚΥΛΛΙΟΠΟΙΗΣΗ ΣΕ ΜΙΓΜΑΤΑ
ΣΥΜΠΟΛΥΜΕΡΩΝ/ΟΜΟΠΟΛΥΜΕΡΩΝ.
ΕΠΙΔΡΑΣΗ ΤΗΣ ΑΡΧΙΤΕΚΤΟΝΙΚΗΣ ΚΑΙ ΤΗΣ ΣΥΣΤΑΣΗΣ

ΚΩΝΣΤΑΝΤΙΝΑ ΚΑΡΑΓΙΑΝΝΗ



ΙΤΕ-ΙΝΣΤΙΤΟΥΤΟ ΗΛΕΚΤΡΟΝΙΚΗΣ ΔΟΜΗΣ ΚΑΙ ΛΕΪΖΕΡ

ΗΡΑΚΛΕΙΟ, ΝΟΕΜΒΡΙΟΣ 2005

Abstract

Micellization in block copolymer/homopolymer blends is investigated via Dynamic Light Scattering and Rheology. The study is performed as a function of the block copolymer composition, architecture and its concentration in the homopolymer matrix. The effect of the total polymer concentration in a non-selective solvent is examined as well. Three (polyisoprene)₂(polystyrene), I₂S, graft copolymers with similar molecular weights but different compositions are utilized in matrix, PI, that is chemically identical to one of the copolymer blocks and the results are discussed in relation to the behavior of linear polyisoprene-polystyrene diblock copolymers, in polyisoprene, in solution and in the bulk.

Micellization of the graft copolymer in the homopolymer matrix is observed for the sample with the highest PS number fraction ($f_{PS}=0.64$) in all copolymer and total polymer concentrations. In contrast, the copolymer/homopolymer blend containing the graft copolymer that is poor in polystyrene ($f_{PS}= 0.09$) indicates no micelle formation. Moreover, on the other hand, blends containing the graft copolymer with intermediate PS content ($f_{PS}=0.32$) exhibit micelle formation depending on the polymer concentration in solution.

The linear diblock copolymers, exhibit similar behavior with the respective graft ones. The copolymer/homopolymer blends containing the rich in polystyrene linear diblock copolymer show micelle formation in all concentrations, whereas the one with intermediate PS content contains micelles only in high polymer concentrations. However, the linear and graft copolymer systems differ on the size of the micelles that they form.

Results from Rheology show no influence on the rheological response of the samples, independently of the presence or absence either of the copolymer chains or of the micelles. The results are discussed in relation to theoretical predictions and results from former works.

Keywords: Micelles, diblock copolymers, graft copolymers, polymeric solutions, polymeric blends, Rheology, Dynamic Light Scattering.

Περίληψη

Στην παρούσα εργασία γίνεται μελέτη της μικυλλιοποίησης σε μίγματα συμπολυμερούς/ομοπολυμερούς μέσω Δυναμικής Σκέδασης Φωτός και Ρεολογίας. Πιο συγκεκριμένα μελετάται η επίδραση της σύστασης του συμπολυμερούς, της αρχιτεκτονικής του και της συγκέντρωσής του σε μήτρα ομοπολυμερούς, καθώς επίσης και η επίδραση της ολικής συγκέντρωσης του πολυμερούς μέσα σε μη επιλεκτικό διαλύτη. Χρησιμοποιούνται τρία εμβολιασμένα συμπολυμερή, παρόμοιου μοριακού βάρους, που έχουν δύο συστάδες πολυισοπρενίου και μία συστάδα πολυστυρενίου (I_2S), αλλά διαφέρουν στη σύσταση. Τα συμπολυμερή αυτά βρίσκονται σε μήτρα πολυισοπρενίου και τα αποτελέσματα των μετρήσεων συγκρίνονται με τη συμπεριφορά γραμμικών δυσυσταδικών συμπολυμερών πολυισοπρενίου-πολυστυρενίου, σε μήτρα πολυισοπρενίου, σε κατάσταση διαλύματος και τήγματος.

Στην περίπτωση του δείγματος εμβολιασμένου συμπολυμερούς, με την μεγαλύτερη συστάδα πολυστυρενίου ($f_{PS}=0.64$), σε μήτρα ομοπολυμερούς παρατηρήθηκε μικυλλιοποίηση σε όλες τις συγκεντρώσεις συμπολυμερούς και πολυμερούς. Αντιθέτως, στο μίγμα που περιέχει το εμβολιασμένο συμπολυμερές με τη μικρότερη συστάδα πολυστυρενίου ($f_{PS}=0.09$) δεν υπάρχει σχηματισμός μικυλλίων. Επιπλέον, τα μίγματα που περιέχουν το συμπολυμερές με ενδιάμεση σύσταση πολυστυρενίου ($f_{PS}=0.32$) εμφανίζουν μικυλλιοποίηση ανάλογα με την ολική συγκέντρωση του διαλύματος.

Τα γραμμικά δυσυσταδικά συμπολυμερή εμφανίζουν παρόμοια συμπεριφορά με τα αντίστοιχα εμβολιασμένα. Τα μίγματα που περιέχουν το “πλούσιο” σε πολυστυρένιο γραμμικό συμπολυμερές, παρουσιάζουν μικυλλιοποίηση σε όλες τις συγκεντρώσεις, ενώ το δείγμα του συμπολυμερές με την ενδιάμεση περιεκτικότητα σε πολυστυρένιο, περιέχει μικύλλια μόνο στις μεγάλες συγκεντρώσεις πολυμερούς. Τα γραμμικά και τα εμβολιασμένα συμπολυμερή διαφέρουν στο μέγεθος των μικυλλίων που σχηματίζουν.

Τέλος, τα αποτελέσματα από τις ρεολογικές μετρήσεις δεν δείχνουν επίδραση στη ρεολογική συμπεριφορά των δειγμάτων, ούτε από την παρουσία συμπολυμερούς ούτε την παρουσία μικυλλίων. Τα αποτελέσματα συγκρίνονται με θεωρητικές προβλέψεις και προηγούμενες δουλειές.

Λέξεις κλειδί: Μικύλλια, δυσυσταδικά συμπολυμερή, εμβολιασμένα συμπολυμερή, πολυμερικά διαλύματα, πολυμερικά τήγματα, Ρεολογία, Δυναμική Σκέδαση Φωτός.

Ευχαριστίες

Τελειώνοντας την διπλωματική μου εργασία στα πλαίσια του μεταπτυχιακού προγράμματος, θα ήθελα να ευχαριστήσω τον καθηγητή μου κύριο Σ. Αναστασιάδη για όλη την βοήθεια που μου προσέφερε τόσο προπτυχιακά όσο και μεταπτυχιακά.

Επίσης θα ήθελα να ευχαριστήσω την δρ. Κ.Χρυσοπούλου για τη συνεχή καθοδήγησή της και τις πολύτιμες συμβουλές της. Δεν θα μπορούσα να ξεχάσω τους Λ. Παπουτσάκη και Μ. Καπνιστό, που με βοήθησαν στην ομαλή διεξαγωγή των πειραμάτων μου.

Ευχαριστώ πολύ τα παιδιά του εργαστηρίου των πολυμερών και κυρίως τους Βασιλική, Δάφνη, Μαρία, Θανάση και Στέλιο για το ωραίο κλίμα συνεργασίας και ένα μεγάλο ευχαριστώ στην οικογένειά μου που είναι δίπλα μου.

CONTENTS

➤ *Chapter 1*

<i>Introduction</i>	1
---------------------------	---

➤ *Chapter 2*

Experimental techniques

2.1 Dynamic Light Scattering.....	16
2.1.1 Electromagnetic theory.....	19
2.1.2 Photon correlation spectroscopy (PCS).....	21
2.1.3 Experimental setup.....	22
2.1.4 Correlator.....	24
2.1.5 Correlation function analysis.....	24
2.2 Rheology.....	28
2.2.1 Static measurements.....	30
2.2.2 Dynamic measurements.....	30
2.3 Materials.....	35
2.3.1 Polymer synthesis.....	35
2.3.2 Sample preparation.....	37

➤ *Chapter 3*

Results and Discussion

A. Dynamic Light Scattering results.....	39
--	----

□ Effect of composition and concentration/Graft copolymer-homopolymer blends

3.1	I ₂ S#1.....	40
3.1.1	I ₂ S#1 0.5wt% in PI.....	40
3.1.2	I ₂ S#1 1wt% in PI.....	43
3.1.3	I ₂ S#1 2wt% in PI.....	45
3.2	I ₂ S#5.....	49
3.2.1	I ₂ S#5 2wt% in PI.....	49
3.2.2	I ₂ S#5 1wt% in PI.....	52
3.2.3	I ₂ S#5 0.5wt% in PI.....	56
3.3	I ₂ S#3.....	59

□ Effect of composition and concentration/Linear copolymer-homopolymer blends

3.4	PS ₃₀ PI ₇₀	64
3.5	PS ₇₀ PI ₃₀	68
3.5.1	PS ₇₀ PI ₃₀ 2wt% in PI.....	68
3.5.2	PS ₇₀ PI ₃₀ 0.5wt% in PI.....	70

B. Rheological results.....73

3.6	Steady measurements.....	73
3.7	Dynamic measurements.....	76
3.7.1	Polyisoprene.....	76
3.7.2	I ₂ S#1 in PI.....	78
3.7.3	I ₂ S#5 in PI.....	80

➤ *Chapter 4*

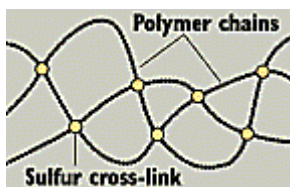
Conclusions and future work.....85

Chapter 1

Introduction

Polymers are defined as macromolecules containing a large number of structural units covalently bonded with each other. In the natural world, polymers have been around since the beginning of time. Proteins, starch, cellulose and rubber all possess polymeric properties.

Natural polymers have been studied since 1800s. Natural rubber from latex became hard and brittle when it got too cold, a sticky mess when it got too warm. In 1839 Charles Goodyear discovered that latex heated with sulfur—or “vulcanized”—would remain elastic at a wide range of temperatures. Carriages, cars, trucks, and buses have traveled billions of miles on tires made from vulcanized rubber and synthetic substitutes.



The world's first widely manufactured plastic (named Bakelite) was created in early 1900s. The commercial success of Bakelite led to more intensive research to understand the chemical structure of polymers. In the 1930's many other plastics were developed, such as poly(vinyl chloride) (PVC), poly(methyl methacrylate) etc.

Today, the polymer industry has grown to be larger than the aluminum, copper and steel industries combined. They have a range of applications that far exceeds that of any other class of material available to man. Current applications extend from adhesives, coatings, foams, and packaging materials to textile and industrial fibers, composites, electronic devices, LCD's screens, biomedical devices, optical devices, and precursors for many newly developed high-tech ceramics.

Block copolymers^(1,2) are a special class of polymeric materials mainly after the development of anionic polymerization which allowed the sequential addition of monomers in living polymeric chains and the synthesis of polymers with very narrow molecular weight distribution, first synthesized in the late 1950's. They are composed of long thermodynamically incompatible sequences ("blocks") of the same monomer unit, covalently bonded to each other. Since the blocks can be connected in a variety of ways complex architectures can be achieved (linear, cyclic, star like, dendrimer, graft etc). Some chosen schematic structures are shown in Figure 1.1.

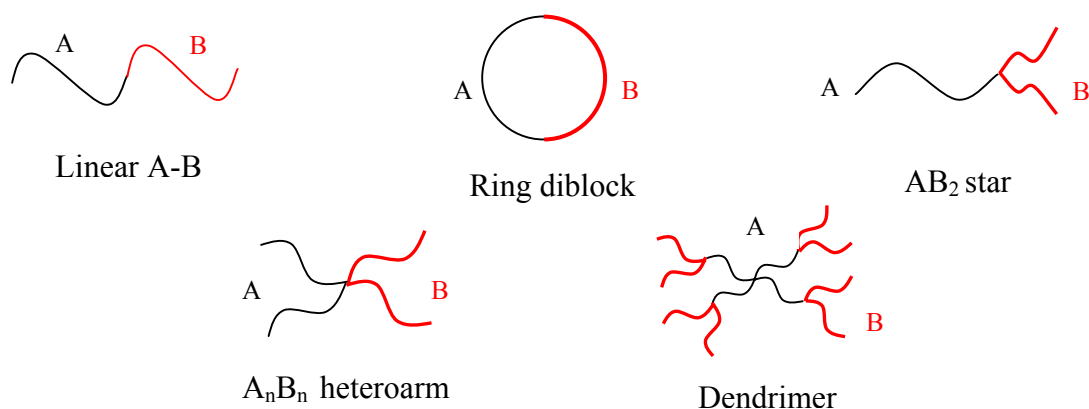


Figure 1.1 Schematic structures for different architectures of block copolymers.

The wide use of block copolymers (from thermoplastic elastomers and high impact plastics to pressure-sensitive adhesives, additives, etc) led to the rapid development of research activity on their synthesis, physical properties and applications. Several laboratories have worked on the properties of block copolymers.

The incompatibility between the sequences of block copolymers gives rise to a rich variety of microstructures in bulk and in solution as shown in Figure 1.2. The length scale of these microstructures is comparable to the size of the block copolymer molecules (typically several nm), therefore the microstructures are highly coupled to the physical and chemical characteristics of the molecules. Parameters that allow customizing the microstructure of block copolymer are the volume fraction of the blocks, f and the chain architecture. Moreover, the Flory-Huggins segmental interaction parameter ($\chi=a+b/T$, $b>0$, T : temperature) of the blocks and the overall degree of polymerization N define the transition from a homogeneous or disordered state toward a microphase-separated state characterized by long range order.⁽³⁻⁵⁾



Figure 1.2 Schematic representations of typical morphologies.

The micellization of block copolymers in a selective solvent (selective is a solvent that is preferentially good for one of the blocks) or in a homopolymer matrix has attracted much attention, on account of their current and potential widespread applications, such as stabilizers, nanoreservoirs, controlled drug delivery, gene therapy, formation of metal nanoparticles etc. Micelles are stable aggregates formed by the self-assembly of amphiphiles or copolymers. Micellization occurs at a fixed temperature above a concentration called the critical micelle concentration (cmc). At higher concentrations, the micelles can order onto a lattice above a critical gel concentration (cgc). These regimes are illustrated in Figure 1.3.

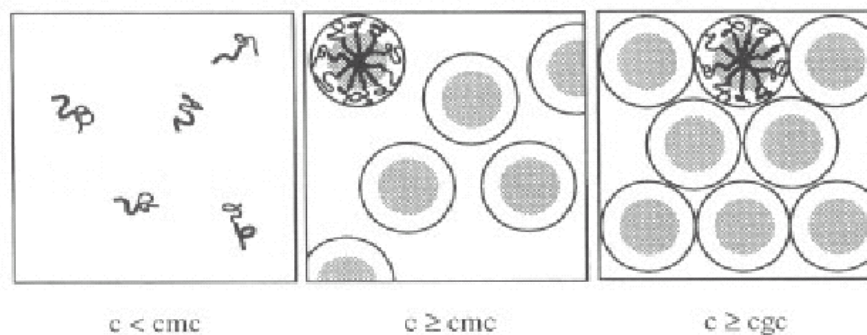


Figure 1.3 Schematic showing the effect of copolymer concentration on the structure of diblock copolymer/homopolymer blends exhibiting spherical micelles.

At a fixed concentration, micellization can occur on changing the temperature above or below the critical micelle temperature (cmt) depending on whether the self-assembly process is endothermic or exothermic. The micellization of block copolymers often occurs via a closed association process, leading to a dynamic equilibrium between micelles with a narrow molar mass and size distribution and dispersed copolymer molecules. The micelle structure depends on the length of the block forming the micellar core with respect to the block forming the corona.⁽²⁾

The size and structure of block copolymer micelles can be obtained from a number of methods. Scattering techniques such as small angle X-ray scattering (SAXS) and small angle Neutron scattering (SANS) are among the most powerful.

Micellization is directly related to segmental incompatibility of the blocks. In fact, under certain conditions of temperature and concentration, when a block copolymer AB is dissolved in a selective solvent, the copolymer chains may associate reversibly to form micellar aggregates. The micelles consist of a more or less swollen core of the insoluble blocks surrounded by a flexible fringe of soluble blocks. These micelles are generally spherical with narrow size distribution but may adopt a variety of shapes the most common being anisotropic ellipsoidal, worm-like or rod-like micelles.⁽⁶⁾

Especially, the addition of a block copolymer in a homopolymer matrix is largely utilized to improve the performance of polymeric materials for many important industrial applications, i.e. as compatibilizers for controlling the morphology (phase structure) in

immiscible polymer blends. In blends of two or more homopolymers with block copolymer, there is an interplay between macrophase separation of the homopolymers and microphase separation of block copolymer, which effect predominates depends on the relative lengths of the polymers and on the composition of the blocks. In binary blends, low molecular weight homopolymer is solubilized within a microphase-separated block copolymer structure at low concentration. Increasing the molecular weight of the homopolymer such that it approaches that of the corresponding block in the copolymer, leads to an increasing tendency for segregation of the homopolymer to the middle of the microdomain. Finally, if the molecular weight of the homopolymer is greater than that of the block copolymer, macrophase separation tends to predominate.

The effectiveness of block or graft copolymers as emulsifiers is determined by their partitioning to the blend interface.⁽⁷⁾ Mixing the additive with one of the components may lead to the formation of copolymeric micelles in the homopolymer matrix.⁽⁸⁾ It may also occur copolymer chain trapping⁽⁹⁾ at the interface.

Several theories have been developed over the years in order to predict the structural parameters of a micelle (cmc, core radius, shell thickness, hydrodynamic radius) as a function of copolymer characteristics, e.g. M_w and composition. The emulsifying behavior of block copolymers at the polymer/polymer interface has attracted the interest of the theoreticians over the last 20 years.⁽¹⁰⁻¹³⁾ Noolandi and Hong⁽¹⁰⁾ utilized their theory of inhomogeneous systems to investigate the segment density profiles at the interface for the system homopolymer A/ homopolymer B/ diblock copolymer A-B/ common solvent. They investigated the effect of the molecular weight and the concentration of the diblock on the interfacial tension under the assumption that the copolymer is either localized at the interface or randomly distributed in the bulk homopolymer phases, i.e. for the concentrations below the critical micelle concentration (cmc). Shull and Kramer⁽¹¹⁾ developed and applied the Noolandi-Hong theory for the samples without solvent, whereas they also discussed the possibility of micelle formation in view of their earlier experimental observations. Semenov⁽¹²⁾ developed an analytical mean-field theory for the equilibrium of the block copolymers in a homopolymer layer between an interface with another homopolymer and the free surface, whereas he also

analyzed the situation for concentrations higher than the cmc and found that the micelles are attracted to both the free surface and to the polymer/polymer interface, but he did not investigate the interfacial tension reduction due to the copolymer segregation to the polymer/polymer interface.⁽¹³⁾

For molecular weights and concentrations when micelles are present, the equilibrium exists between homogeneously distributed copolymer and copolymer in the micelle. The density of the absorbed chains, σ , is determined by equating the chemical potential of the copolymer chains in the bulk and copolymer chains in a micelle:⁽¹²⁾

$$\mu_{mic}(N) = \mu_{bulk}(\phi; N) \quad (1.1)$$

which also determines the volume fraction ϕ of copolymers remaining homogeneously distributed in the bulk. In the cases of copolymers in mixture of homopolymers, someone has to take into account the chemical potential of the interface.

The free energy density of a homogeneous mixture of an A-B copolymer with an A homopolymer is:

$$\frac{F_{bulk}}{k_B T} = \frac{\phi}{N} \ln\left(\frac{\phi}{e}\right) + \frac{1-\phi}{e} + \chi\phi f(1-f\phi) \quad (1.2)$$

Thus the chemical potential of a copolymer chain homogeneously distributed in the bulk, $\mu_{bulk} = N[(1-\phi)\partial F_{bulk} / \partial\phi + F_{bulk}]$ is:

$$\frac{\mu_{bulk}}{k_B T} = \ln\phi - \phi - (1-\phi)\frac{N}{P_A} + \chi f N(1-2f\phi + f\phi^2) \quad (1.3)$$

where ϕ is the copolymer volume fraction in the A-rich homopolymer phase.

Leibler⁽¹³⁾ considered monodisperse spherical micelles formed by Q_m diblock copolymer A-B chains added to a B homopolymer. In this case, A blocks make the core with radius R_A whereas the B blocks form the corona. The free energy of the micelle is represented by a sum of three contributions:

$$F_{mic} = A\gamma_o + F_{core} + F_{corona} \quad (1.4)$$

where $A=4\pi R_A^2$ is the interfacial area, γ_0 is the A/B interfacial tension. The equilibrium value of Q_m is obtained by minimizing the free energy. The chemical potential for a A-B diblock copolymer in a micelle within homopolymer B is:^(11,12)

$$\frac{\mu_{mic}^{spherical}}{k_B T} = (3/2)^{4/3} f_A^{4/9} (1.74 f_A^{-1/3} - 1)^{1/3} (\chi N)^{1/3} \quad (1.5)$$

where f_A is the volume fraction of the A block, χ is the Flory-Huggins interaction parameter and N is the number of segments of the copolymer.

This procedure presented by Leibler, was extended by Lyatskaya et al⁽¹⁴⁾ for spherical micelles of simple graft copolymers AB_2 in a B homopolymer, where the chemical potential is:

$$\frac{\mu_{mic}^{spherical}}{k_B T} = (3/2)^{4/3} f_A^{4/9} (4.74 f_A^{-1/3} - 4)^{1/3} (\chi N)^{1/3} \quad (1.6)$$

which it was written that is valid only for $f_A \leq 0.5$.

In addition to the theories, computer simulations have been developed in order to consider aspects of block copolymer self-association, such as the chain length dependence, the dynamics of chain exchange between micelles, the formation of surface micelles etc.⁽²⁾ Also, quite a number of models have been created for the analysis of the scattering data from micellar systems and the characteristics of the micelles.⁽¹⁵⁻¹⁷⁾

Several groups have worked on the investigation of micellization in mixtures of diblock copolymers in homopolymer matrix. One of the first reported work on the quantitative study of the structure of block copolymer micelles in homopolymer solution was performed by Selb et al.⁽¹⁸⁾ in 1983. These authors performed small angle neutron scattering (SANS) on dilute mixtures of poly(styrene-butadiene) diblock copolymers, having deuterated polystyrene blocks, in low molecular weight (1600 to 6500) polybutadiene homopolymer. The structure proposed for all blends was that of spherical micelles in which the core, made up of the d-polystyrene blocks, was surrounded by a shell of polybutadiene blocks, which were highly swollen in a matrix of homopolybutadiene. It was found that the core radius increased with the molecular

weight of the polystyrene block and decreased with the increasing molecular weight of the polybutadiene block. In addition, the core radius increased with increasing molecular weight of the homopolybutadiene matrix and decreased with copolymer concentration.

The micelle formation in blends of polystyrene-polybutadiene diblock copolymer and polybutadiene homopolymer have also been studied by Rigby and Roe.⁽¹⁹⁾ These authors utilized small angle X-ray scattering to investigate the effect of temperature and copolymer concentration on the micelle structure of a copolymer with molecular weight $M_w=25000$, containing 52wt% polystyrene, in a small molecular weight polybutadiene. Copolymer concentrations between 0.5- 8% were studied. The micelles were assumed to consist of spherical polystyrene core surrounded by a shell of polybutadiene block swollen with homopolymer. The radius of gyration of the micelle cores was found to increase slightly with copolymer concentration and rapidly as the temperature was increased above 60°C. The latter was attributed to the swelling of the micelle core with homopolymer and the eventual dissolution of the micelles. In addition, increasing the temperature above 60°C also caused the cmc to increase rapidly.

Another study by these authors⁽²⁰⁾ examined the effect of the relative block lengths on the micelle structure. Blends containing polystyrene-polybutadiene copolymers of similar molecular weight but different composition (containing 25, 50 or 75wt% polystyrene) in a low molecular weight polybutadiene, were examined. Spherical micelles were assumed for all blends, although electron microscopy was not performed to confirm this. Quantities that were evaluated are: the average core radius, the polydispersity of core radius, the cmc, the degree of swelling of the core with homopolymer, as well as the number density of micelles and the apparent hard sphere radius of interaction. It was found that at room temperature the cmc increased drastically upon increasing the polybutadiene content in the copolymer, whereas the size of the micelles of a given copolymer was found to be independent of concentration.

The effect of temperature on the radius of gyration of the core was qualitatively similar, for all three copolymers, to the results of their previous study⁽¹⁹⁾, except that the temperature at which the radius of gyration abruptly increased was seen to increase with increasing polystyrene content in the copolymer. Also, the radius of the core increased

with the molecular weight of the polystyrene block and the cmc increased with temperature. Finally, the calculated volume fraction of homopolymer in the micelle core increased steadily with temperature for all three copolymers, whereas the ratio of the effective hard sphere micelle radius to the average core radius was found to decrease as the polybutadiene content in the copolymer decreased.

Further study⁽³⁾ of a number of well characterised polystyrene-polybutadiene block copolymers and polystyrene matrices were employed so that the effect of polystyrene and polybutadiene block molecular weights, polystyrene homopolymer molecular weight and copolymer concentration on the micellar structure could be investigated. In these systems, transmission electron microscopy could be performed due to the glassy state of polystyrene at room temperature, unlike the previous studies for which the liquid-like nature of the homopolymer at room temperature did not favour it. This allowed an identification of micelle geometry. They observed changes in micelle morphology from spherical to nonspherical geometries by changing the butadiene block fraction or the homopolymer molecular weight.

The viscoelastic properties of such systems attracted the scientific interest, as well. Watanabe and co workers^(21,22) carried out systematic rheological studies on polystyrene-b-polybutadiene diblock copolymers in a low molecular weight polybutadiene (hB). As long as the PS-b-PB content was low, a Newtonian behavior was obtained in the region of low frequency. However, when the copolymer content exceeds a certain critical value, the blend exhibits a plateau in the low-frequency tails of the storage, G' , and the loss, G'' , moduli. This plateau was called a second plateau and was related to some slow relaxation process existing in the system. Blends of polystyrene-polyisoprene diblock copolymers in PI matrix were studied also with dielectric spectroscopy taking advantage of the dipole moment of PI block that have dipoles in the I blocks and the dielectric behavior could be examined.⁽²³⁾ The micelles were found to exhibit both fast and slow relaxation, similar to the relaxation of star polymers. The fast process corresponds to the relaxation of individual PI blocks tethered on the PS cores. The slow process was attributed to the Stokes-Einstein diffusion of the micelles.

Recently, work has been directed toward understanding the effect of the addition of symmetric diblock copolymer additives on the reduction of the interfacial tension between two immiscible homopolymers using surface tensiometry and more precisely the technique of axisymmetric pendant drops profile. The work was performed as a function of molecular weight, M_w , and concentration, Φ_{add} , of the additive.⁽²⁴⁾ They observed that at low N 's (number of segments of the copolymer) the interfacial tension reduction increased with increasing N , whereas above a certain additive M_w the interfacial tension increased by further increasing N as shown in Figure 1.4(a). The change of the behavior for high copolymer molecular weight was understood by considering the possibility of micelle formation.

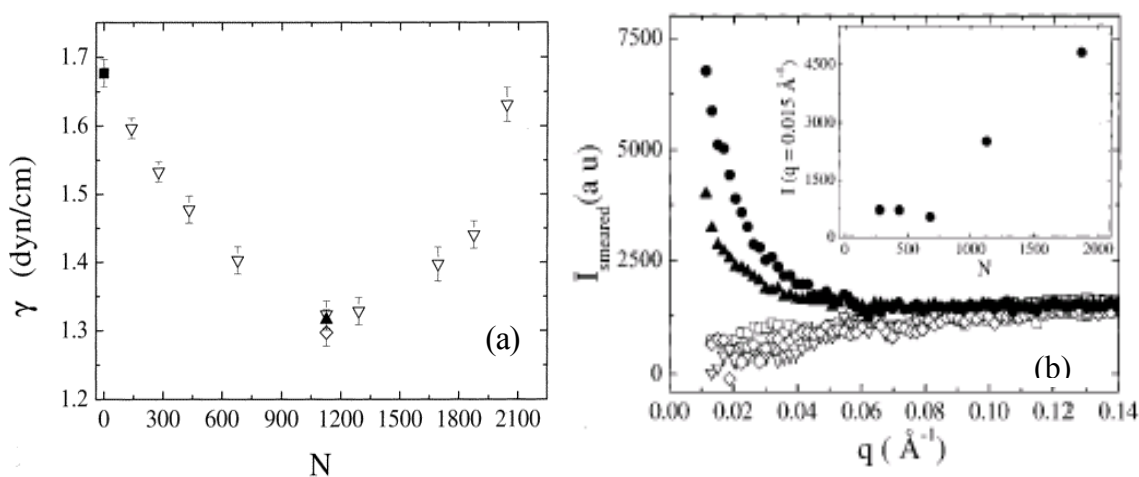


Figure 1.4 (a) Interfacial tension for PS/PS-*b*-PI/PI systems as a function of the number of copolymer segments N at 140°C and 2wt% copolymer added to the polystyrene phase (∇), added to polyisoprene (\blacktriangle) and when 1wt% was added to polystyrene and 1wt% to polyisoprene (\diamond). (b) Small angle X-ray scattering intensity for 2wt% blends of the various diblocks in the polyisoprene homopolymer at 140°C as a function of the scattering vector q . The inset shows the scattering intensity at $q = 0.015 \text{\AA}^{-1}$ as a function of N .

These assumptions were supported by the SAXS measurements shown in Figure 1.4(b), where it was noted that the scattering intensity was very low for the diblocks with low M_w (low N 's) whereas it was significantly increased for high M_w 's. This dependence

of I on N signifies the presence of micelles in the blends with diblocks of high molecular weight and their absence for low molecular weight additives.

Changing molecular architecture, making graft copolymers for instance, control of the morphology and phase behavior unobtainable with linear diblock architecture at the same volume fractions can be produced. Several years ago a group⁽²⁵⁾ studied the morphologies of a series of well-defined I_2S simple graft block copolymers via SAXS and transmission electron microscopy. They found that the volume fraction windows in which specific strongly segregated micro-phase separated morphologies are observed are shifted to higher volume fractions of PS graft material than in the corresponding linear diblocks and came in good agreement with theoretical⁽²⁶⁾ phase behavior.

Theoretical phase behavior for simple graft, A_2B , block copolymers has been calculated by Milner⁽²⁷⁾ and experimental results were in good agreement with that.⁽²⁵⁾ In addition the micellization of the copolymer, is expected to influence the flow behavior of the sample, as it was shown in former investigation of linear diblock copolymers.⁽²⁸⁾

The effects of molecular architecture on the static behavior have been considered several years ago.⁽²⁹⁾ Solutions in neutral good solvents have been used to complement the investigations on diblock copolymers. In contrast, dynamic behavior of block copolymers much later has attracted the scientific interest.⁽³⁰⁾

A series of (polyisoprene)₂(polystyrene), I_2S , and (polystyrene)₂(polyisoprene), S_2I , graft copolymers was used to investigate the effect of the macromolecular architecture and composition, f , of the block copolymer additives on the interfacial tension between two immiscible homopolymers using the technique of axisymmetric pendant drops profile.⁽³¹⁾ A decrease in interfacial tension, followed by a levelling off (plateau) was observed, as well, as the copolymer concentration (Φ_{add}) increased. In these results, the interfacial tension in the plateau regime is lower than that for symmetric diblock with the same molecular weight. A dependence on the copolymer composition, was observed that was attributed to the micellar formation for some of the graft copolymers. When I_2S graft copolymer was added to PI homopolymer, there was no micelles formed for high values of f_{PI} and the copolymer chains at the interface were at equilibrium with chains homogeneously mixed within the PI phase. In the specific

work,⁽³¹⁾ theoretical calculations were performed in the case of both A-B linear diblock copolymers and AB₂ graft copolymers within a B homopolymer. The size of the micelles, R, as well as the number of copolymer chains per micelle, Q_m, were calculated. In the case of spherical micelles the radius R of the micelles and the radius R_A of the micelle core are given by:

$$R = \left(\frac{3}{4\pi}\right)^{1/3} (Q_m N b^3)^{1/3} \quad \text{and} \quad R_A = \left(\frac{3}{4\pi}\right)^{1/3} (Q_m f_A N b^3)^{1/3} \quad (1.7)$$

where N is the degree of polymerization, f_A is the composition of the A block and b is the segmental length, for both linear and graft copolymers. Following the minimization of the free energy, the number of copolymer chains per micelle, Q_m, is calculated for the linear copolymer:

$$Q_m = \left(\frac{3}{2}\right)^{1/2} \left(\frac{4\pi}{3}\right) \chi^{1/2} N f_A^{2/3} (1.74 f_A^{-1/3} - 1)^{-1} \quad (1.8)$$

and for the graft copolymer:

$$Q_m = \left(\frac{3}{2}\right)^{1/2} \left(\frac{4\pi}{3}\right) \chi^{1/2} N f_A^{2/3} (4.74 f_A^{-1/3} - 4)^{-1} \quad (1.9)$$

These works were the motivation for the current investigation. The same graft copolymer/homopolymer systems were utilized in order to probe the dependence of copolymer architecture on micelle formation using dynamic light scattering and to study the rheological response of the different systems.

In the current work we present an investigation of the micelle formation in diblock copolymer/ homopolymer blends as a function of copolymer architecture, composition and concentration. Three different (polyisoprene)₂(polystyrene) graft copolymers⁽³²⁾ in homopolymer have been used and the data are discussed in relation to the behavior of linear polyisoprene-polystyrene diblock copolymers in the same homopolymer matrix. We have performed measurements in the bulk and in (the neutral good solvent) toluene solutions for different copolymer concentrations and for a range of total polymer concentrations.

The graft copolymers used have similar molecular weights, they differ though on the polystyrene (PS) content (f_{ps}). The measurements have been carried out mainly using Dynamic Light Scattering (Photon Correlation Spectroscopy) with additional rheological measurements. A dependence of the micellization on the PS content is observed. For *copolymers with high f_{ps}* , micelle formation occurs in all copolymer and total polymer concentrations with the micelle's size being independent of copolymer concentration, predicted also from thermodynamic theories.^(8,17) On the contrary, *copolymers with low f_{ps}* do not indicate micelle formation in any of the investigated copolymer concentrations. Remarkably interesting is the behavior of the *copolymers with $f_{ps}=0.32$* that show a total polymer concentration dependent micelle formation. Moreover, the investigation of the linear copolymer/homopolymer blends confirmed the effect of the relative block lengths on the micellization. A dependence of the rheological behavior on the presence of micelles was not observed probably due to the low copolymer concentrations. More specifically, the results for the polyisoprene, mixture of polyisoprene with the graft copolymer with low PS content and polyisoprene with the graft copolymer that forms micelles, showed similar viscosities and dynamic behavior.

References

- (1) Legge, R.; Holden, N. R.; Schroeder, H. E. Eds.; Hansen Publishers, Thermoplastic Elastomers-A Comprehensive Review, Munich **1988**
- (2) Hamley, I. W. The Physics of Block Copolymers, Oxford, Oxford University Press **1998**
- (3) Kinning, D. J.; Thomas, E.; Fetters, L. J.; J. Chem. Phys. **1989**, *90*, 5806
- (4) Bates, F. S.; Fredricson, G. H. Annu. Rev. Phys. Chem. **1940**, *41*, 525
- (5) Leibler, L. Macromolecules **1980**, *13*, 1602
- (6) Riess, G. Prog. Polym. Sci. **2003**, *28*, 1107 and references therein
- (7) Fayt, R.; Jérôme, R.; Teyssié, Ph. J. Polym. Sci., Polym. Lett. Ed. **1986**, *24*, 25. Green, P. F.; Russell, T. P. Macromolecules **1991**, *24*, 2931. Dai, K. H.; Kramer, E. J. J. Polym. Sci., Part B; Polym. Phys. **1994**, *32*, 1943

-
- (8) Whitmore, M. D.; Noolandi, J. *Macromolecules* **1985**, *18*, 657
- (9) Duke, T. A. J. Ph.D. Dissertation, University of Cambridge, Cambridge, U.K., **1989**
- (10) Noolandi, J.; Hong, K. M. *Macromolecules* **1982**, *15*, 482; *1984*, *17*, 1531; Noolandi, J. *Polym. Eng. Sci.* **1984**, *24*, 70
- (11) Shull, K. R.; Kramer, E. J. *Macromolecules* **1990**, *23*, 4769
- (12) Semenov, A. N. *Macromolecules* **1992**, *25*, 4967
- (13) Leibler, L. *Macromol. Chem., Macromol. Symp.* **1988**, *16*, 1; *Physica A* **1991**, *172*, 258
- (14) Lyatskaya, J.; Balazs, A. C.; Gersappe, D. *Macromolecules* **1995**, *28*, 6278; Lyatskaya, J.; Gersappe, D. Gross, N. A.; Balazs, A. C. *J. Phys. Chem.* **1996**, *100*, 1449
- (15) Pedersen, J. S.; Svaneborg, C. *Curr. Opin. Colloid Interface Sci.* **2002**, *7*, 158 and references therein
- (16) Castelletto, V.; Hamley, I. W. *Curr. Opin. Colloid Interface Sci.* **2002**, *7*, 167
- (17) Mayes, A. M.; Olvera de la Cruz, M. *Macromolecules* **1988**, *21*, 2543
- (18) Selb, J.; Marie, P.; Rameau, A. Duplessix, R. and Gallot, Y. *Polym. Bull.* **1983**, *10*, 444
- (19) Rigby, D.; Roe, R. J. *Macromolecules* **1984**, *17*, 1778
- (20) Rigby, D.; Roe, R. J. *Macromolecules* **1986**, *19*, 721
- (21) Watanabe, H.; Kotaka, T.; Hashimoto, T.; Shibayama, M.; Kawai, H. *J. Rheol.* **1982**, *26*, 153, Watanabe, H.; Koataka, T. *Polym. J.* **1982**, *14*, 739; **1983**, *15*, 337; *J. Rheol.* **1983**, *27*, 223
- (22) Watanabe, H.; Sato, T.; Osaki, K. *Macromolecules* **1996**, *29*, 104
- (23) Sato, T.; Watanabe, H.; Osaki, K. and Yao, M.L. *Macromolecules* **1996**, *29*, 3881
- (24) Retsos, H.; Margiolaki, I.; Messaritaki, A.; Anastasiadis, S. H. *Macromolecules* **2001**, *34*, 5295
- (25) Pochan, D. J. et al *Macromolecules* **1996**, *29*, 5091; *Macromolecules* **1996**, *29*, 5099
- (26) Bates, F. S.; Berney, C. V.; Cohen, R. E. *Macromolecules* **1983**, *16*, 1101

- (27) Milner, S. T. *Macromolecules* **1994**, *27*, 2333
- (28) Watanabe, H.; Yao, M. L.; Sato, T.; Osaki, K. *Macromolecules* **1997**, *30*, 5905
- (29) Olvera de la Cruz, M.; Sanchez, I. C. *Macromolecules* **1986**, *19*, 2501
- (30) Anastasiadis, S. H.; Chrissopoulou, K.; Fytas, G. et al *Macromolecules* **1997**, *30*, 2445; Chrissopoulou, K.; Harville, S.; Anastasiadis, S. H.; Fytas, G.; Mays, J. W.; Hadjichristidis, N. *Polym. Phys.* **1999**, *37*, 3385
- (31) Retsos, H.; Anastasiadis, S. H.; Pispas, S.; Mays, J. W.; Hadjichristidis, N. *Macromolecules* **2004**, *37*, 524
- (32) Pispas, S.; Hadjichristidis, N.; Potemkin, I.; Khokhlov, A. *Macromolecules* **2000**, *33*, 1741

Chapter 2

Experimental Techniques

2.1 Dynamic light scattering

Electromagnetic radiation is one of the most important probes of the structure and dynamics of matter. The absorption of light has provided detailed information about electronic, vibrational and rotational energy levels of molecules and has enabled the physicists and chemists to determine the structure of complex molecules. When photons impinge on a molecule they can either impart energy to (or gain energy from) the translational, rotational, electronic and vibrational degrees of freedom of the molecules. They thereby suffer frequency shifts. Thus the frequency spectrum of the scattered light will exhibit resonances at the frequencies corresponding to these transitions.

When light impinges on matter, the electric field of the light induces an oscillating polarization of the electrons in the molecules. The molecules then serve as secondary source of light and scatter light. The frequency shifts, the angular distribution, the polarization and the intensity of the scattered light are determined by the size, shape and the molecular interactions in the scattering material. Thus from the light scattering characteristics of a given system it should be possible, with the aid of the theory of time

dependent statistical mechanics and electromagnetism, to obtain information about the structure and molecular dynamics of the scattering medium.⁽¹⁾

Light scattering can be characterized as inelastic or elastic, whether there is frequency shift of the incident light or not, respectively. The elastic scattering is called Rayleigh scattering. Rayleigh scattering comes from the translational and rotational degrees of freedom, while vibrational degrees of freedom give Raman scattering. The development of laser techniques has made possible the measurement of very small frequency shifts in the light scattered from matter. Additionally, because of the high intensities of laser sources, it is possible to measure even weakly scattered light.

Rayleigh, Mie, Smoluchowski, Einstein, and Debye developed the basic theory of light scattering in the beginning of the twentieth century. Light scattering was first studied experimentally by Tyndall⁽²⁾ and then theoretically by Rayleigh.⁽³⁾ These studies concerned scattering from assemblies of noninteracting particles, sufficiently small compared to the wavelength of the light, to be regarded as point dipole oscillators. Rayleigh explained the blue color of the sky and the red sunset as due to the preferential scattering of the blue light by the molecules in the atmosphere.

Although Rayleigh had developed a theory of light scattering from gases with some success, it was found that the intensity of scattering by condensed phases was less than that predicted by his formula by more than one order of magnitude. This effect was correctly attributed to the destructive interference between the wavelets scattered from different molecules. Smoluchowski and Einstein^(4,5) elegantly circumvented this difficulty by considering the light to be a continuous medium in which thermal fluctuations give rise to local inhomogeneities and thereby to the intensity and concentration fluctuations. These authors developed the fluctuation theory of light scattering. According to this theory, the intensity of the scattered light can be calculated from the mean square fluctuations in density and concentration that in turn can be determined from macroscopic data such as the isothermal compressibility and the concentration dependence of the osmotic pressure. The intensity of the light is thus obtained without considering the detailed molecular structure of the medium. This approach to light scattering has played a very important role in the theory of light scattering.

Dynamic light scattering examines the relaxation of the fluctuations giving us information in reciprocal space for the spatial Fourier length $2\pi/q$, where q is the scattering vector. This length is related to a characteristic time, which is the time that the particle needs to travel the distance $2\pi/q$. In general, if there are no interactions, the slow motions are depicted in the low q regime, whereas the fast ones are shown in the high q regime.

In a light-scattering experiment, light from a laser passes through a polarizer to define the polarization of the incident beam and then impinges on the scattering medium. The scattered light then passes through an analyzer, which selects a given polarization and finally enters the detector. The position of the detector defines the scattering angle θ . In addition, the intersection of the incident and the scattered beam defines a scattering region of volume V for each θ . This is illustrated in Figure 2.1

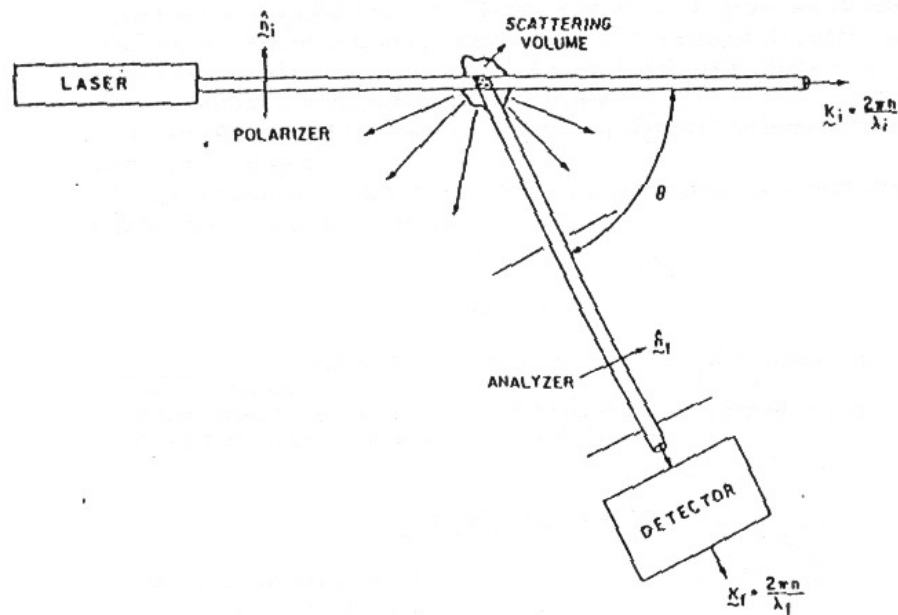


Figure 2.1 Typical experimental setup for light scattering experiment.

The quantity measured in a dynamic light scattering experiment is the time-dependence of the scattered intensity $I(t)$. Because of the continuous movement of the molecules, their position changes and the scattered intensity fluctuates. The fluctuations

of $I(t)$ are connected with the motion of the scatterers, that is characterized by the diffusion coefficient D .

2.1.1 Electromagnetic theory

The theory of light scattering can be developed on the basis of quantum field theory. The major results of this theory differ little from classical theory of light scattering, so for the purposes of this work we will discuss only the classical theory.

Consider a nonmagnetic, nonconducting, nonabsorbing medium with average dielectric constant ϵ_0 and refractive index $n = \sqrt{\epsilon_0}$. Let the incident electric field be a plane wave of the form

$$\vec{E}_i(\vec{r}, t) = \hat{n}_i E_o \exp i(\vec{k}_i \vec{r} - \omega_i t) \quad (2.1)$$

where \hat{n}_i is a unit vector in the direction of the incident electric field; E_o is the field amplitude; \vec{k}_i is the propagation vector and the ω_i is the angular frequency.

This plane wave is incident upon a medium that has a local dielectric constant

$$\vec{\epsilon}(\vec{r}, t) = \epsilon_0 \vec{I} + \delta\vec{\epsilon}(\vec{r}, t) \quad (2.2)$$

where $\delta\vec{\epsilon}(\vec{r}, t)$ is the dielectric constant fluctuation tensor at position \vec{r} and time t and \vec{I} is the second-rank unit tensor.

It can be shown that the component of the scattered electric field at a large distance R from the scattering volume with polarization \hat{n}_f , propagation vector \vec{k}_f , and frequency ω_f is

$$E_s(R, t) = \frac{E_o}{4\pi R \epsilon_0} \exp(ik_f R) \int_V d^3 r \exp[i(\vec{q} \cdot \vec{r} - \omega_f t)] [\hat{n}_f \cdot [\vec{k}_f \times (\vec{k}_f \times (\delta\vec{\epsilon}(\vec{r}, t) \cdot \hat{n}_i))]] \quad (2.3)$$

where the subscript V indicates that the integral is over the scattering volume. The vector \vec{q} is defined in terms of the scattering geometry as $\vec{q} = \vec{k}_i - \vec{k}_f$ where \vec{k}_i and \vec{k}_f point, in the directions of propagation of the incident wave and of the wave that reaches the

detector respectively. This is illustrated in Figure 2.2. The angle between \mathbf{k}_i and \mathbf{k}_f is called the scattering angle θ .

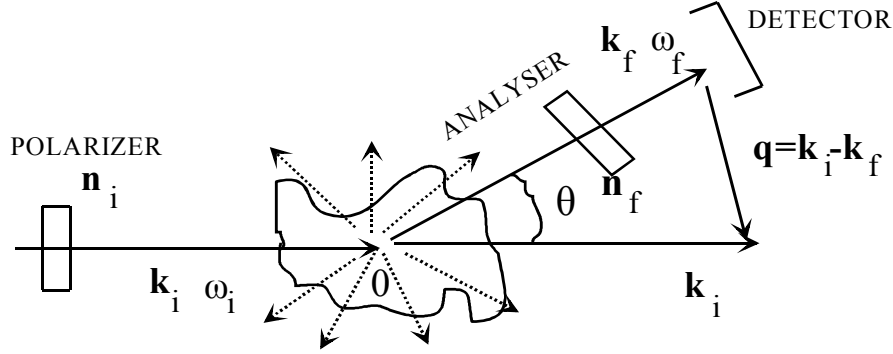


Figure 2.2 Light of polarization \mathbf{n}_i and wave vector \mathbf{k}_i is scattered in all directions. Only scattered light of wave vector \mathbf{k}_f and polarization \mathbf{n}_f arrives at the detector. The scattering vector $\vec{q} = \vec{k}_i - \vec{k}_f$ is defined by the geometry.

The magnitude of \vec{k}_i and \vec{k}_f are respectively $2\pi n/\lambda_i$ and $2\pi n/\lambda_f$ where λ_i and λ_f are the wavelengths of the incident and scattered radiation and n is the refractive index of the scattering medium. It is usually the case that the wavelength of the incident light changes very little in the scattering process so that $|\vec{k}_i| \cong |\vec{k}_f|$ and the scattering vector is

$$q^2 = |\vec{k}_i - \vec{k}_f|^2 = k_i^2 + k_f^2 - 2\vec{k}_i \cdot \vec{k}_f = 2k_i^2 - 2k_i^2 \cos \theta = 4k_i^2 \sin^2 \left(\frac{\theta}{2} \right) \Rightarrow \quad (2.4)$$

$$q = 2k_i \sin \left(\frac{\theta}{2} \right) = \left(\frac{4\pi n}{\lambda_i} \right) \sin \left(\frac{\theta}{2} \right)$$

This is the Bragg condition. It specifies the wave vector component of the dielectric constant fluctuations that will give rise to scattering at an angle θ .

Spatial Fourier transform of the dielectric fluctuations $\delta\vec{\epsilon}(\vec{q}, t) = \int_V d^3r \exp[i(\vec{q} \cdot \vec{r})] \delta\vec{\epsilon}(\vec{r}, t)$ and equation 2.3 give:

$$E_s(R, t) = \frac{-k_f^2 E_o}{4\pi R \epsilon_o} \exp[i(k_f R - \omega_f t)] \delta\epsilon_{if}(q, t) \quad (2.5)$$

where

$$\delta\varepsilon_{if}(\vec{q}, t) \equiv \vec{n}_f \cdot \delta\vec{\varepsilon}(\vec{q}, t) \cdot \vec{n}_i \quad (2.6)$$

is the component of the dielectric constant fluctuation tensor along the initial and final polarization directions. The time-correlation function of the electric field is:

$$\langle E_s^*(R, 0)E_s(R, t) \rangle = \frac{k_f^4 |E_o|^2}{16\pi^2 R^2 \varepsilon_o^2} \langle \delta\varepsilon_{if}(\vec{q}, 0)\delta\varepsilon_{if}(\vec{q}, t) \rangle \exp(-i\omega_f t) \quad (2.7)$$

and the spectral density of scattered light is

$$I(\vec{q}, \omega_f, \mathbf{R}) = \left[\frac{|E_o|^2 k_f^4}{16\pi^2 R^2 \varepsilon_o^2} \right] \frac{1}{2\pi} \int_{-\infty}^{\infty} dt \langle \delta\varepsilon_{if}(\vec{q}, 0)\delta\varepsilon_{if}(\vec{q}, t) \rangle \exp[i(\omega_f - \omega_i)t] \quad (2.8)$$

Equation (2.8) indicates the inverse λ^4 and R^2 dependence of the characteristics of any spherical wave. The λ^4 dependence is related to the observation that the blue light is scattered more than red light. It also indicates that radio waves would not be scattered as much as visible light. As a consequence of the larger scattering intensities, it is much easier to perform scattering experiments with visible light than with longer wavelength infrared or radio waves. It should be also noted that equation (2.8) is an expression for the light spectral density in terms of dielectric constant fluctuations. In a medium that dielectric constant does not fluctuate the light is scattered only in the $q=0$ direction.

Nowhere in this treatment was it necessary to determine the explicit dependence of the dielectric fluctuations on molecular properties. The above theoretical expression is purely phenomenological. Any attempt to write this formula in molecular terms will necessarily involve some degree of approximation, nevertheless, it will contribute significantly in our intuitive understanding of light scattering and will be useful for practical applications.

2.1.2 Photon correlation spectroscopy (PCS)

In a photon correlation spectroscopy experiment the measured quantity is the normalized autocorrelation function of the scattered intensity $G(q, t)$, in the polarized ($G_{VV}(q, t)$) or depolarized ($G_{VH}(q, t)$), geometry:

$$G(q, t) = \frac{\langle I(q, t)I(q, 0) \rangle}{\langle I(q, 0) \rangle^2} \quad (2.9)$$

Polarized geometry gives us information about the fluctuations of the concentration or the density of the material, while the depolarized one gives us information regarding the fluctuations of the orientation of the molecules. Only the polarized geometry has been used in this thesis. The quantity related with the dynamic response of the system is the autocorrelation function of the scattered electric field, $g(q, t)$. The two autocorrelation functions are related via Siegert's⁽¹⁾ relation:

$$G(q, t) = 1 + f^* (\alpha g(q, t))^2 = 1 + f^* |C(q, t)|^2 \quad (2.10)$$

where f^* is a spatial coherence factor that depends on the experimental setup and is connected with the scattered volume and the number of coherence areas⁽⁶⁾ included. The factor α is the fraction of the scattered intensity that relaxes in times that can be measured with PCS. The advantage of the photon correlation spectroscopy is its large time scale (10^{-6} - 10^3 s) giving the ability to separate different relaxation processes.

2.1.3 Experimental setup

The experimental setup, used for the PSC experiments of this work, is shown in Figure 2.3. Scattering angles between 150° - 11° ($q=3.42 \times 10^{-2}$ - $3.4 \times 10^{-3} \text{ nm}^{-1}$) can be measured. The laser is Nd-YAG with a monochromatic beam at 532 nm (Adlas DPY 315II). The maximum power is ~42-52 mW and the diameter of the beam was 0.32 mm (TEM_{00}). The incident beam passes through optics (two mirrors M1, M2 and a polarizer P1 and a lens F1) before it impinges in the sample. The intensity and position of the beam are continuously recorded by a four Photo Diode system (PD). The sample is filtered in an optical glass cell of 10 mm in diameter, which is placed in a bath that contains toluene for refractive index matching. The scattered beam passes through an optical system of a lens and two pinholes H1 and H2 before it impinges the amplifier. The lens is $2f/2f$ and is

placed in a distance equal to $2f$ from the scattering volume and the second pinhole H2 respectively. The amplifier is a photomultiplier (THORN EMI). The two pinholes H1 and H2 (0.3mm diameter) define the scattering volume. The two polarizers P1 and P2 define the polarization of the beam. The incoming beam is always polarized perpendicular to the scattering plane while P2 can be rotated so that both vertically (V) and horizontally (H) polarized components are accessible. The bath temperature which is also the sample temperature, is controlled by the circulation of a thermostatic liquid (mixture of water and glycol) by means of a thermostat. Temperatures between 10°C – 50°C can be used. A Bus Controller RS-232C device controls the goniometer. A computer, embedded with an electronic correlation card, controls the whole setup. The software used is ALV-5000/E. Details regarding the photon correlator are given in the next paragraph.

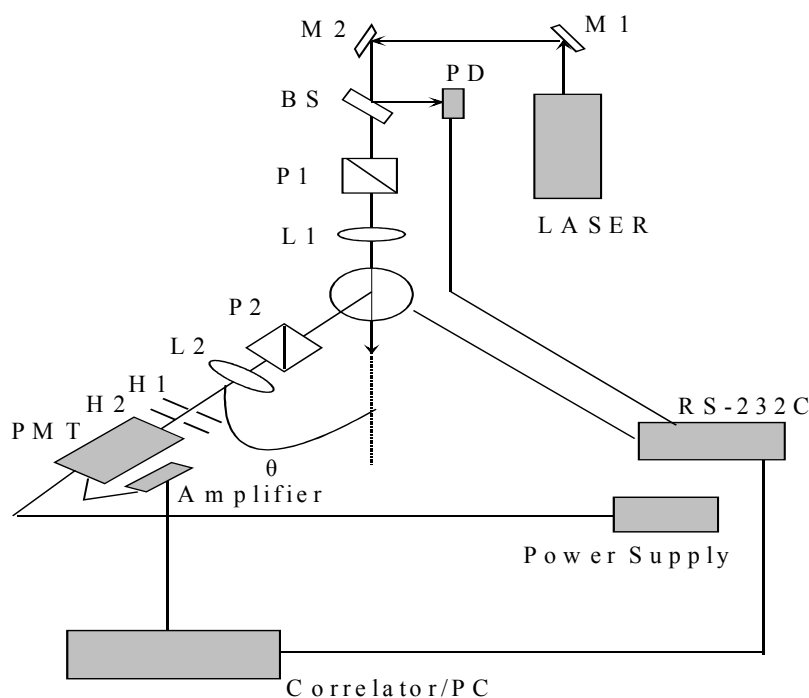


Figure 2.3 The experimental setup used for photon correlation spectroscopy experiments.

2.1.4 Correlator

The correlator is the most important device of the photon correlation spectroscopy setup. It comprises of an electronic card that calculates the correlation function of an electronic signal as following^(7,8):

- a) First, it counts the photoelectronic pulses $n(t)$, during a storage time t_s (sample time), during the real time t of the experiment
- b) Second, it lags the samples for integer multiplies of the sample time $\tau=kt_s$ (lag time)
- c) Next, it multiplies the real and time results with the lag time
- d) Finally, it sums the products

From the above $n(q, t+\tau)n(q, t)$ is calculated over the duration of the whole measurement, for different values of τ while the photon correlation function is also calculated:

$$G(\tau) = \langle n(t+\tau)n(t) \rangle = \lim_{T \rightarrow \infty} \frac{1}{T} \int_{-T}^T n(t+\tau)n(t) dt \quad (2.11)$$

which can be approximated by:

$$G(\tau) = \sum_{i=0}^{N-1} n_i n_{i+k} \quad (2.12)$$

Normalization of the above equation gives:

$$G_{norm}(q, t) = \frac{\langle n(q, t)n(q, 0) \rangle}{\langle n(q, 0) \rangle^2} \quad (2.13)$$

The photon correlator, used in this study, is an ALV-5000 Multi Tau Digital Correlator with 280 channels which can makes 2×10^9 multiplies/sums per second.⁽⁷⁾

2.1.5 Correlation function analysis

The correlation function of a solution of PS in toluene (weight fraction $w=0.0043$) is shown in Figure 2.4 (a). The above-mentioned experimental setup was used for this

measurement. The correlation function of Figure 2.4 (a) is described with a simple exponential decay and can be fitted with a function of the form $C(q,t) = \alpha e^{-t/\tau}$, which gives the intensity ($\propto \alpha$) and the relaxation time τ .

In most cases measured correlation function is not as simple as described above but gives more than one relaxation processes. The CONTIN analysis^(9,10) has to be used in order to analyze the correlation function. CONTIN assumes that $C(q,t)$ is a superposition of exponentials, performs an inverse Laplace transform and calculates the distribution of the relaxation times:

$$C(q,t) = \int_{-\infty}^{\infty} L(\ln \tau) \exp(-t/\tau) d(\ln \tau) \quad (2.14)$$

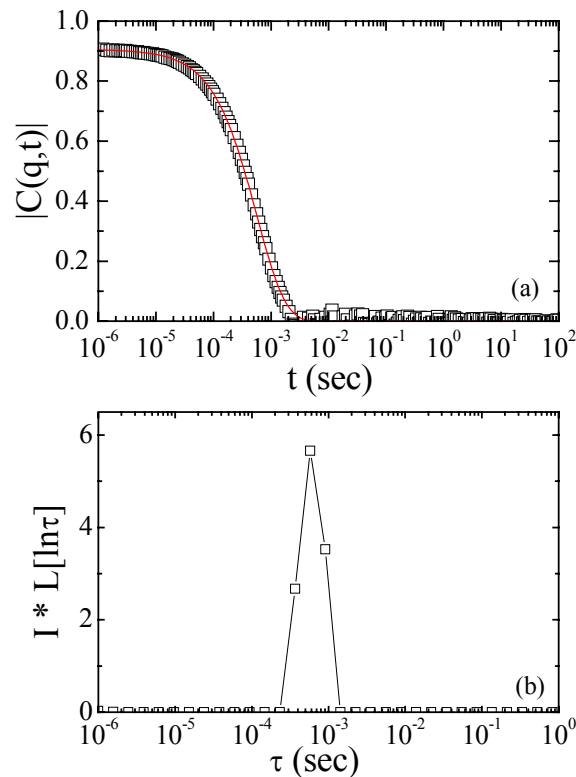


Figure 2.4 (a) Correlation function of polystyrene in toluene $w=0.0043$ at scattering angle $\theta=30^\circ$. (b) The relaxation time distribution multiplied by the normalized intensity. Continues red line on the correlation function is the fit of CONTIN to the correlation function.

After choosing the best fitting of CONTIN, a Gaussian fit was performed to each process of the distribution of relaxation times with the aid of Origin 7 graph and analysis software as shown in Figure 2.5. The parameters of the fit are shown in the inset where x_c is the \ln of the *relaxation time* and A is the area under the curve of the process at the specific angle. The area under the peak multiplied by the normalized scattered intensity calculates *the intensity of the process* from the equation:

$$I(\theta) = \frac{\bar{I}(\theta)}{I_{tol}(\theta)} \cdot \frac{A}{\sqrt{f^*}} \quad (2.15)$$

where $\bar{I}(\theta)$ is the mean intensity at θ angle, $I_{tol}(\theta)$ is the toluene intensity at θ angle and f^* is the spatial coherence factor that in our experiments can be calculated using a standard polystyrene solution in toluene and is given by the form:

$$f^* = \frac{A}{(1 - (1 - \phi)I_{tol} / I_{PS/tol})^2} \quad (2.16)$$

ϕ is the volume fraction of polystyrene in solution.

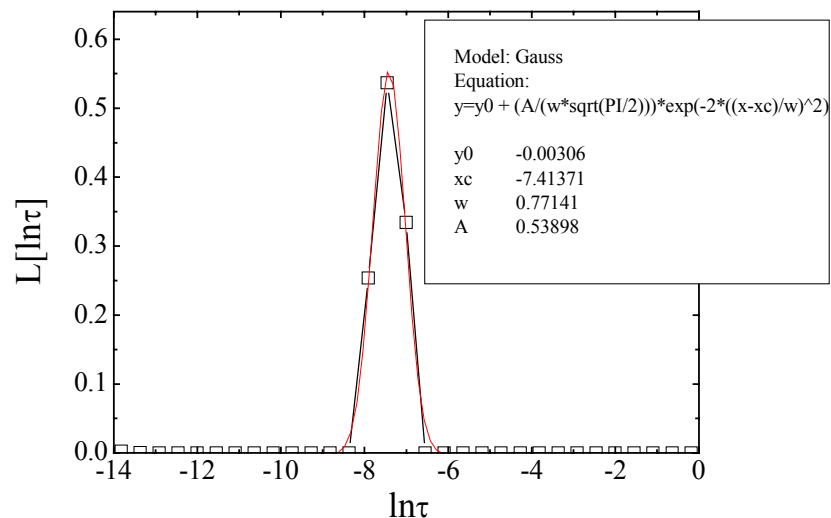


Figure 2.5 Distribution of relaxation times for a PS/tol solution at $w=0.0043$ and $\theta=30^\circ$. The line represents a Gaussian fit.

Another method to analyze the correlation function is the Kolhhrusch-Williams-Watts (K.W.W.)⁽¹¹⁾ function fit, which is described for one relaxation process as:

$$C(q, t) = \alpha e^{-(t/\tau)^\beta} \quad (2.17)$$

and for multiple relaxation processes as:

$$C(q, t) = \sum_{i=1}^n \alpha_i e^{-(t/\tau_i)^{\beta_i}} \quad (2.18)$$

where the sum is over all relaxation processes and β is the exponentiality parameter. For $\beta=1$ the relaxation is exponential and the relaxation time of the process is τ , while for $\beta < 1$ or $\beta > 1$ the average relaxation time is calculated from the equation:

$$\tau(q) = \frac{\tau_{KWW}}{\beta} \Gamma\left(\frac{1}{\beta}\right) \quad (2.19)$$

where $\Gamma(x)$ is the Γ -function.

A typical KWW fit is shown in Figure 2.6, where the parameters used are also shown in the inset.

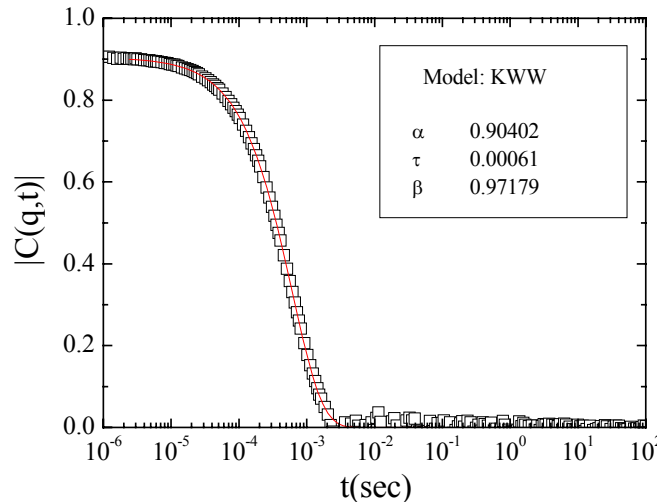


Figure 2.6 Correlation function of polystyrene solution in toluene in weight fraction $w=0.0043$ and at scattering angle $\theta=30^\circ$. Continues red line on the correlation function is the KWW fit. In the inset the parameters used for this fit are shown.

Either with the Contin analysis or with a fit with KWW we can find the characteristic relaxation time τ of the process for each angle. The relaxation rate of the process is calculated for each angle, from equation:

$$\Gamma = \frac{1}{\tau} \quad (2.20)$$

For a diffusive process, the characteristic graph of Γ versus q^2 can be fitted with a line that corresponds to equation:

$$\Gamma = D \cdot q^2 \quad (2.21)$$

where D is the diffusion coefficient and is calculated from the slope of the fit. In dilute solutions, the diffusion coefficient and the hydrodynamic radius R_h are related by the Stokes Einstein⁽¹²⁾ equation:

$$R_h = \frac{kT}{6\pi\eta D} \quad (2.22)$$

where η is the viscosity of the solvent, k is the Boltzmann constant and T is the temperature of the sample.

In the cases that $R_g q \ll 1$, the scattered intensity on the wave-vector can be fitted with Guinier equation:

$$I(q) = I_o \cdot e^{-\frac{R_g^2 q^2}{3}} \quad (2.23)$$

where R_g is the radius of gyration of the scatterer.⁽¹³⁾

2.2 Rheology

Rheology is the study of the deformation and flow of a material in response to an applied stress. Simple solids store energy and provide a spring-like, elastic response, whereas simple liquids dissipate energy through viscous flow. For more complex viscoelastic materials, rheological measurements reveal both the solid-and fluid-like responses and generally depend on the time scale at which the sample is probed.⁽¹⁴⁾

A “rheometer” measures the rheological properties of a complex liquid as a function of *rate* or *frequency* of deformation. The simplest devices impose a *shearing flow* on the sample and measure the resulting stress, or alternatively, impose a shearing stress and measure the resulting shearing rate. This can be achieved in several geometries like the plane Couette geometry, the parallel plate or the cone and plate geometry etc.⁽¹⁵⁾ Specifically, the parallel plate and the Couette geometry are shown schematically in a drawing in Figure 2.7.



Figure 2.7 Schematic representation of (a) the Couette and (b) parallel plate geometry

When a force is applied to a volume of material (Figure 2.8) then a displacement (deformation) occurs. If two plates (area, A), separated by fluid distance (separation height, H) apart, are moved (at velocity V by a force, F) relative to each other, Newton's law states that the shear stress (the force divided by area parallel to the force, F/A) is proportional to the shear strain rate (V/H). The proportionality constant is known as the (dynamic) viscosity (η).

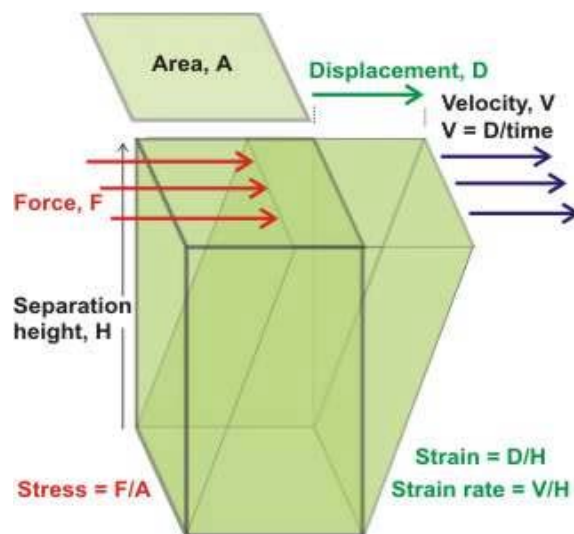


Figure 2.8 Schematic representation of a sample's displacement

The effect (shear strain τ) is quantified by the displacement per unit height (D/H) and the rate of this effect (strain rate $\dot{\gamma}$) is the velocity per unit height (V/H), where the height is the distance to a relatively unaffected position. The viscosity η is the tendency of the fluid to resist flow and is defined by:

$$\eta = \frac{\text{shear stress}}{\text{shear rate}} (\text{Pa} \cdot \text{s}) \quad (2.24)$$

One way to characterize the rheological response of a system is to measure the rate of deformation (static measurements). Another way is to measure the shear modulus as a function of frequency (dynamic measurements).

2.2.1 Static measurements

In each geometry, the steady shear rate imposed on the fluid depends on a driving velocity and the dimensions of the geometry. For the sliding plate, which is used in these experiments, the shear rate, $\dot{\gamma}$, is the velocity V of the moving plate divided by the gap, l , between the two plates, hence $\dot{\gamma} = V/l$. The shear stress, τ , is the force that a flowing liquid exerts on a surface per unit area of that surface, in the direction parallel to the flow. The shear viscosity, η , is then defined as

$$\eta = \frac{\tau}{\dot{\gamma}} \quad (2.25)$$

After a steady shearing flow has been imposed on a fluid for a suitable period of time, the shear stress often comes to a steady state, which depends on the imposed shear rate $\dot{\gamma}$. The ratio of the steady shear stress τ to the shear rate $\dot{\gamma}$ is then the steady state shear viscosity η .

2.2.2 Dynamic measurements

Another way to explore the rates of structural rearrangement within a complex fluid, that does not significantly deform the fluid's microstructure, is to impose small-amplitude oscillatory shearing. This kind of deformation can be achieved in a parallel plate geometry, as the one shown in Figure 2.9, by rotating the bottom-plate about its axis

with an angular velocity that oscillates sinusoidally $\Omega(t) = \Omega_0 \cos(\omega t)$, where ω is the frequency of oscillation, in units of radians per second. The shear rate $\dot{\gamma} = \frac{d\gamma}{dt}$ is a sinusoidal function of time $\dot{\gamma} = \Omega r/h$ and so is the shear strain $\gamma = (\Omega_0 r/\omega h) \sin(\omega t) = \gamma_0 \sin(\omega t)$. The ratio $\gamma_0 = \Omega_0 r/\omega h$ is the strain amplitude, the amplitude of the displacement of the sliding plate.

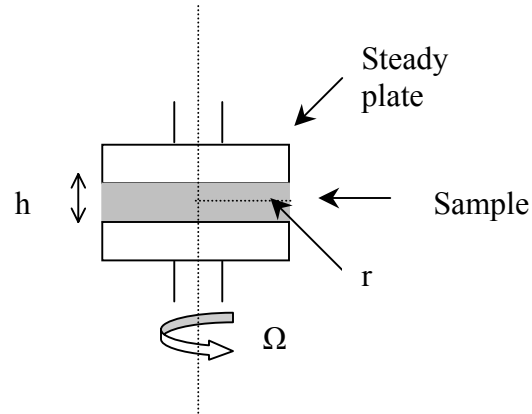


Figure 2.9 Schematic representation of a rheometer in the parallel plate geometry.

If the strain amplitude γ_0 is small enough that the fluid structure is not much disturbed by the deformation, then the stress measured during the oscillatory deformation is controlled by the rates of spontaneous rearrangements, or relaxations present in the fluid in the quiescent or equilibrium state. The shear stress $\tau(t)$ produced by a small-amplitude deformation is proportional to the amplitude of the applied strain γ_0 and is itself sinusoidally varying in time. The maxima and minima of the sinusoidally varying stress signal are not necessarily coincident with the maxima and minima in the strain. In general, the sinusoidally varying stress can be represented as

$$\tau(t) = \gamma_0 [G'(\omega) \sin(\omega t) + G''(\omega) \cos(\omega t)] \quad (2.26)$$

$G'(\omega)$ is in phase with the strain and is called the storage modulus, while $G''(\omega)$ is in phase with the rate of strain $\dot{\gamma}$ and is called the loss modulus. The storage modulus

represents storage of elastic energy, while the loss modulus represents the viscous dissipation of that energy. When the ratio G''/G' is high ($\gg 1$) the material is liquid-like, but if the ratio is low ($\ll 1$) the material is solid-like. The storage and loss moduli G' and G'' for typical liquid-like and solid-like fluids are shown in Figure 2.10. For the liquid-like fluid, the storage modulus is much lower than the loss modulus and it scales with frequency as $G' \sim \omega^2$, the loss modulus is linear in frequency $G'' \sim \omega$. The low-frequency “liquid-like” region in which G' and G'' obey these power laws is called the *terminal region*. For the “solid-like” fluid, $G' \gg G''$, and G' is nearly frequency independent. The small amplitude shear strain regime where the shear stress is given by equation 2.27, is called *linear viscoelastic regime*.⁽¹⁴⁾

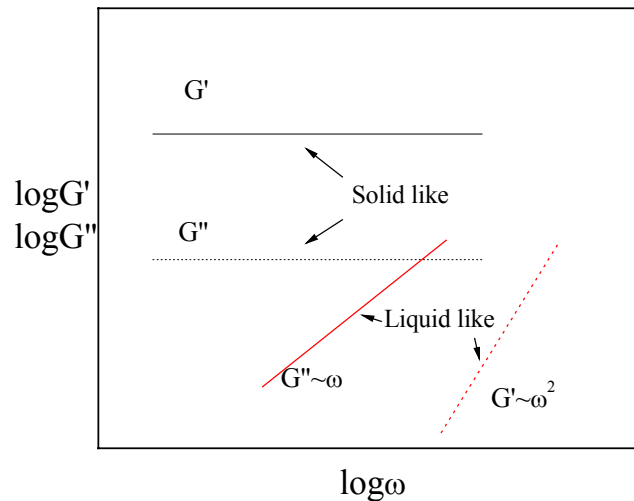


Figure 2.10 Illustration of frequency dependent storage and loss moduli G' and G'' for prototypical “liquid-like” and “solid-like” materials.

The main advantage of the above rheological experiment arises from the spectroscopic character. The experimental time to get a data point is almost equal to $2\pi/\omega$. Hence, this allows us to measure specific relaxation processes with time constants in the order of $1/\omega$, independently of other slow or fast relaxation processes that may occur in the system.

In the present work, a strain-controlled rheometer has been utilized. With this rheometer, one can settle the strain and measure the stress. Both static and dynamic

measurements have been performed, in order to study the rheological behavior of our samples and to investigate the influence of the presence of micelles. For the static measurements, we performed *steady rate sweep*, where for different shear rates, the viscosity of the sample was determined (eq. 2.25).

Furthermore, three different dynamic measurements have been carried out for each sample, in each temperature. First were performed *dynamic time sweep* measurements, at a certain shear strain and frequency. If the values of G' and G'' were constant, this suggested that the sample had reached the equilibrium state. Then *dynamic strain sweep* experiments were carried out, where the loss and the storage moduli were measured as a function of strain at different fixed frequencies, so that the strain regime can be determined, in which the sample has a linear viscoelastic behavior. Finally, once the linear viscoelastic region was determined and the equilibrium of the sample was ensured, *dynamic frequency sweep* experiments were performed on the sample, as a function of frequency, at a fixed strain. The values of the calculated loss and storage moduli indicated the behavior of the sample. As mentioned above, with this technique the rates of structural rearrangement, can be investigated.

Since most rheometers can only cover a few decades of frequency at any temperature, the frequency range could be extended using the time-temperature superposition (TTS).⁽¹⁴⁾ This procedure is based on the fact that relaxation times and the corresponding moduli G' , G'' depend on the absolute temperature T . On a log-log plot, a frequency shift by a_T that does not change the shape of the curves $G'(\omega)$ and $G''(\omega)$ is performed. The curves are also shifted equally along the modulus axis through their dependence on T and viscosity ρ . The shift along the modulus axis is often small or negligible, however, since when T increases, ρ decreases by thermal volume expansion, and this effect at least partially cancels the direct effect of T on modulus. Thus, the curves $G'(\omega)$ and $G''(\omega)$ measured at different temperatures can be superposed by shifting along the logarithmic frequency axis ($a_T\omega$), with a minor shift along the logarithmic modulus axis ($b_T G'$, $b_T G''$), if desired.

A curve with data from multiple temperatures superposed onto a single line is called a *master curve*. At the reference temperature T_{ref} to which the data have been shifted, one has by definition $a_T=1$. Since $a_T \ll 1$ at temperatures well above T_{ref} and $a_T \gg 1$ when $T \ll T_{ref}$, the master curve typically covers a much wider range of effective frequencies than are covered by experiments at any single temperature.

This procedure (TTS) is appropriate for many polymer melts and solutions, as long as there are no phase transitions or other temperature-dependent structural changes in the liquid. Time-temperature superposition also works for dilute solutions, as long as there are not large temperature-dependent changes in solvent quality. Fluids for which linear rheological data, such as G' and G'' , superimpose at different temperatures are said to be thermorheologically simple.

In our measurements, the data have been time-temperature superposed by shifting along the horizontal log frequency axis by amount, a_T , required to bring the data into superposition. The shift along the vertical axis has been performed using shift factor b_T that has the form:

$$b_T(T) = \frac{\rho(T_{ref}) \cdot T_{ref}}{\rho \cdot T} \quad (2.28)$$

where ρ is the viscosity of the sample and T the temperature.⁽¹⁶⁾

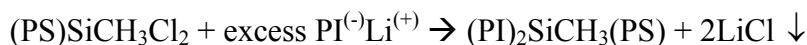
2.3 Materials

2.3.1 Polymer synthesis

A series of (polyisoprene)₂(polystyrene), I₂S, 3-microarm star block copolymers (simple grafts) were synthesized by anionic polymerization using a high-vacuum technique in glass reactors provided with breakseals for the addition of reagents and constrictions for removal of products; the chlorosilane chemistry approach was utilized. Synthesis and characterization on these systems have been described elsewhere.^(17,18,19) Following standard purification of the monomers, the solvent, and the methyltrichlorosilane linking agent, the living polystyrenyllithium (PSLi) and polyisoprenyllithium (PILi) living arms were synthesized in benzene solution using sec-butyllithium as the initiator. The following reactions describe the steps of the polymerization.



and




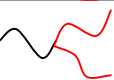
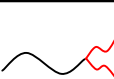
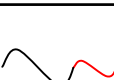
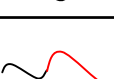
The reaction of a solution ~3% w/v of (PS)Li in benzene with an excess (SiCl/Li=100) of methyltrichlorosilane (CH₃SiCl₃) followed by a removal of the unreacted linking agent; next, an excess of PILi was added to a solution of the macromolecular difunctional linking agent, PS-Si(CH₃)Cl₂, to obtain the CH₃Si(PS)(PI)₂ 3-microarm star copolymers I₂S. The excess PILi was deactivated with degassed methanol. Fractionation of the samples was performed by addition of methanol to a 1% solution of the polymers in a 60/40 benzene/hexane mixture; usually three fractionations were enough to remove any unlinked polyisoprene arms as monitored by size exclusion chromatography. The molecular characteristics of the samples obtained by low-angle

laser light scattering (M_w), size exclusion chromatography SEC (polydispersity), and UV analysis (styrene content) are shown in Table 2.1.

In Table 2.1 and in the following, f_{ps} denotes the number fraction of polystyrene, which constitutes the backbone of the graft copolymer. The polystyrene-polyisoprene linear diblocks ($PS_{30}PI_{70}$ and $PS_{70}PI_{30}$), that have been also used, were synthesized under high vacuum in a glass-sealed apparatus at room temperature using benzene as the solvent and *sec*-BuLi as the initiator with styrene being polymerized first. After the completion of the reaction for both blocks, the living ends were neutralized with degassed methanol. Their molecular characteristics obtained as before are given in Table 2.1 as well. The calculation of the segment's number, N , was based on the average segmental volume. Note that in the I_2S and in the PS-PI samples the polystyrene sequence is perdeuterated (styrene- d_8).

The polyisoprene homopolymer (PI) was synthesized anionically under argon atmosphere by K. Hong and kindly provided to us. Its characteristics are shown in table 2.1 as well.

Table 2.1 Molecular Characteristics of I_2S Graft & PS-PI Diblock Copolymers

	PS PI	M_w	w_{PS}	N^a	f_{ps}
$I_2S\#1$		91300	0.10	1149	0.09
$I_2S\#3$		89 800	0.35	1093	0.32
$I_2S\#5$		87400	0.67	1017	0.64
$PS_{70} PI_{30}$		116 300	0.678	1351	0.65
$PS_{30} PI_{70}$		99 500	0.316	1217	0.29
PI		4000	0	50	0

a. Calculated based on average segmental volume.

2.3.2 Sample preparation

All samples consist of three ingredients, the copolymer, the homopolymer and the solvent (toluene HPLC, LAB-SCAN Analytical Sciences). First the copolymer was diluted in toluene under magnetic stirring. The appropriate amount of PI that was calculated to give the desired copolymer concentrations, was then added. After 24 hours of stirring, to ensure the homogeneity of the sample, the final solution was either filtered through 0.2 μ m Millipore filters into dust free light scattering cells, for the DLS experiments, or utilized for the rheological measurements. Since most of the samples were initially prepared at about 50wt% total polymer concentration in toluene, higher concentrations were achieved by slow evaporation of the solvent to ensure equilibrium.

References

- (1) Berne, B.; Pecora, R. *Dynamic light scattering*, Willey, Interscience Publications, New York **1976**
- (2) Tyndall, J. *Phil. Mag.* **1869**, 37, 364. Tyndall, J. *Phil. Mag.* **1869**, 38, 156
- (3) Rayleigh, Lord, *Phil. Mag.* **1899**, 47, 375. Rayleigh, Lord, *Proc. Roy. Soc.*, **1910**, 484, 25. Rayleigh, Lord, *Proc. Roy. Soc.*, **1914**, 490, 219. Rayleigh, Lord, *Proc. Roy. Soc.* **1918**, 449, 296
- (4) Schmoluchowski, M. *Ann. Phys.* **1908**, 25, 205
- (5) Einstein, A. *Ann. Phys.* **1910**, 33, 1275
- (6) Ford, N. C. Jr. *LightScattering Apparatus in Dynamic Light Scattering in Applications of Photon Correlation Spectroscopy*, Pecora, R. ed. Plenum Press, New York **1985**
- (7) ALV-5000, Multiple Tau Digital Correlator. User's Reference Manual
- (8) Schatzel, K. *Single-photon correlation techniques in Dynamic Light Scattering. The Method and Some Applications*. Brown, W. ed. Oxford University Press **1993**
- (9) Provencher, S. W. *Computer Physics Communications* **1982**, 27, 213; **1982**, 27, 229
- (10) Provencher, S. W. *Macromol. Chem.* **1979**, 180, 201

- (11) Brereton, M. G.; Fischer, E. W.; Fytas, G.; Marschall, U. J. *Chem. Phys.* **1987**, *86*, 4768; Wang, C. H.; Zhang, X. Q. *Macromolecules* **1995**, *28*, 2288
- (12) De Gennes, P.G. *Scaling Concept in Polymer Physics*, Cornell University Press Ithaca, New York **1979**
- (13) Guinier, A.; Fournet, G. *Small Angle Scattering of X-rays*, Wiley **1955**
- (14) Larson, R. G. *The Structure and Dynamics of Complex Fluids*, Clarendon Press, Oxford **1999**.
- (15) Barnes, H.A. *A handbook of elementary Rheology*, University of Wales **2000**
- (16) Ferry, J. D.; Wiley, J. and Sons ed. *Viscoelastic Properties of Polymers*, University of Wisconsin **1980**
- (17) Pochan, D.J.; Gido, S.P.; Pispas, S.; Mays, J.W.; Ryan, A.J.; Fairclough, J.P.A.; Hamley, I.W.; Terill, N.J. *Macromolecules* **1996**, *29*, 5091
- (18) Pochan, D.J.; Gido, S.P.; Pispas, S.; Mays, J.W. *Macromolecules* **1996**, *29*, 5099
- (19) Anastasiadis, S. H.; Chrissopoulou, K.; Fytas, G.; Fleischer, G.; Pispas, S.; Pitsikalis, M.; Mays, J. W.; Hadjichristidis, N. *Macromolecules* **1997**, *30*, 2445.

Chapter 3

Results and Discussion

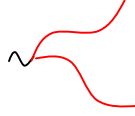
A. Dynamic Light Scattering

All Dynamic Light Scattering (DLS) measurements were carried out using the technique of Photon Correlation Spectroscopy (PCS). The auto-correlation function of the scattered intensity $C_{vv}(q,t) = \langle I(q,t)I(q,0) \rangle / \langle I(q,0) \rangle^2$, in the polarized geometry was measured for angles 30° - 150° ($q = 9.2 \times 10^{-3}$ - $3.4 \times 10^{-2} \text{ nm}^{-1}$). For the samples with very high scattered intensity (e.g. when micelles are present), an absorber was used to reduce the intensity reaching the detector. This reduction has been taken into account by measuring the standard (toluene) at the same conditions. Details for the experimental setup, the measurements and the analysis of the data are given in Chapter 2. All measurements were performed at 293K.

The samples were initially prepared at ~50wt% total polymer concentration in toluene and filtered through 0.2 μm Millipore filters into dust free light scattering cells (outer diameter 10-12mm). Higher concentrations (up to the bulk) were achieved by slow evaporation of the solvent (in vacuum) to ensure the equilibrium and were determined by weighting the resulting solutions.

□ Effect of composition and concentration/ Graft copolymers-homopolymers blends

3.1 I₂S#1 in PI



The first sample that has been studied is a mixture of the graft copolymer I₂S#1, which is the one with the lower composition in polystyrene ($f_{PS}=0.09$) with polyisoprene, PI (Table 2.1, Chapter 2). Three different copolymer concentrations in PI were prepared, 0.5, 1 and 2wt%, in order to study whether there is an effect of copolymer concentration on the micelle formation.

3.1.1 I₂S#1 0.5wt% in PI

The first measurement that has been performed was for the lower total polymer concentration, specifically 50wt% in toluene. The autocorrelation functions of the scattered intensity for different scattering angles are shown in Figure 3.1.

From this Figure we observe that in all angles, the autocorrelation functions have very low contrast and consist of multiple relaxation processes. This is obvious from their shape, which is broader than a single exponential. The lines are fits with superposition of exponentials. Moreover, it is clear that as the scattering angle decreases, the relaxation of the sample becomes slower.

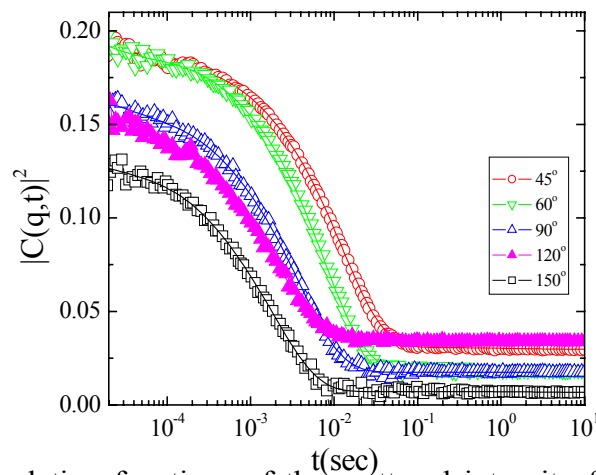


Figure 3.1 Autocorrelation functions of the scattered intensity for different scattering angles of 0.5wt% I₂S#1 in PI, in 50wt% concentration in toluene. Lines are fits with superposition of exponential functions.

The analysis of these data led to the results shown in Figure 3.2. Namely, there are two relaxation processes, both diffusive, since the relaxation rate is of the form $\Gamma \propto q^2$.

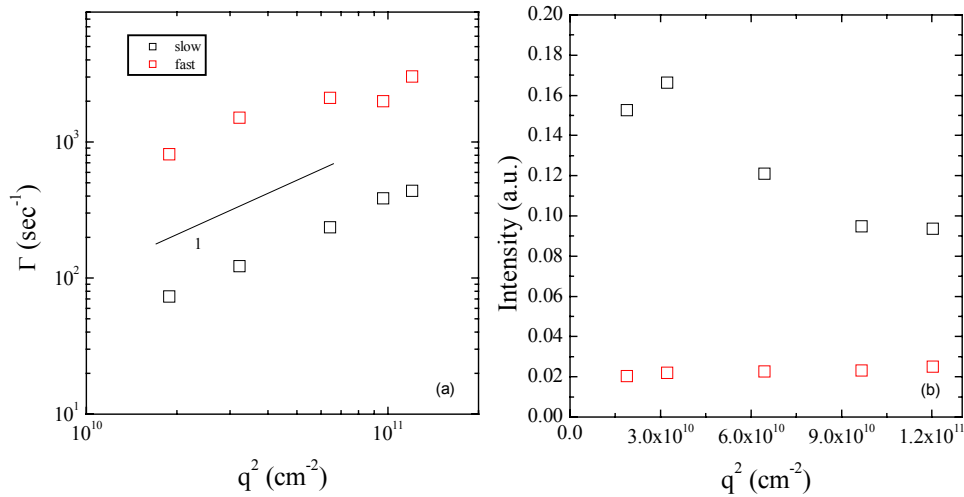


Figure 3.2 Wavevector dependence of (a) the relaxation rate and (b) the scattered intensity of the two relaxation processes for 0.5wt% I₂S#1 in PI, in 50wt% total polymer concentration. The line shows the q^2 dependence.

The fast process has a q -independent intensity, of about 0.02 a.u. Comparing its diffusion coefficient ($D_{\text{fast}} \sim 4 \cdot 10^{-8}$ cm²/sec) with that of former works of the same copolymer in toluene solution⁽¹⁾ we assume that it corresponds to the diffusion of the chains in the PI matrix. For this comparison the difference in the viscosity has been taken into account. The second process is diffusive as well, with $D_{\text{slow}} \sim 5 \cdot 10^{-9}$ cm²/sec but its intensity shows a dependence on the wavevector; it increases with the decrease of the scattering angle and has been associated with the “long range density fluctuations” extensively investigated in both molecular and macromolecular glass formers⁽²⁾ and observed in diblock copolymer melts⁽³⁾ and solutions.⁽⁴⁾

The investigation of 0.5wt% I₂S#1 in PI went on with the study of different total polymer concentrations up to the bulk. In every concentration studied, two relaxation processes were present exhibiting the behavior described above for 50wt% in toluene. A

fast diffusive process with q -independent intensity and a slow diffusive process with amplitude that increases with decreasing scattering angle. The diffusion coefficient together with the intensity of these two processes in all measured concentrations in toluene are shown for scattering angle $\theta = 90^\circ$ in Figure 3.3.

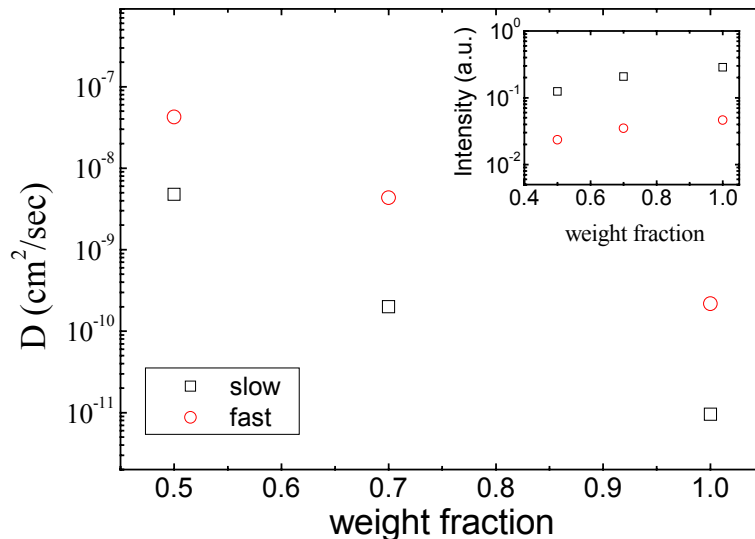


Figure 3.3 Concentration dependence of 0.5wt% I₂S#1 in PI for 90° scattering angle of the diffusion coefficients for the two processes. In the inset the concentration dependence of the scattered intensity for the two processes is shown.

We observe that as the concentration increases, the diffusion coefficient decreases almost three orders of magnitude, a fact that could be related to the increase of the viscosity (from $0.014 \text{ Pa} \cdot \text{s}$ to $3 \text{ Pa} \cdot \text{s}$). So this leads to slower relaxation times, probably because of the fact that the diffusion of the chains becomes more difficult. Furthermore, there is a change in the intensities of these two processes that increase (inset) with the concentration. Once more, the comparison of the diffusion coefficient in all concentrations with those found for the solution of the same copolymer shows that the fast process seems to be the self-diffusion of the polymer chains and the slow process is associated with the “long range density fluctuations”.

3.1.2 I₂S#1 1wt% in PI

Since in the 0.5wt% I₂S#1 in PI sample, there was no indication of micelle formation, further study of this block copolymer has been carried out in a higher copolymer concentration that is 1wt% in PI, again for total polymer concentrations from 50wt% in toluene till the bulk state. The results for an intermediate concentration, specifically 72wt% in toluene, are shown in Figure 3.4 that follows.

From this measurement, it is clear that again there are more than one relaxation processes, since for all angles the autocorrelation functions are not single exponential. These processes have low intensities (Figure 3.5), with the fast process being q -independent, whereas the slow one shows q -dependent intensity. Additionally, we observe that the characteristic relaxation times become slower as the scattering angle decreases. If we attempted to calculate sizes from these diffusion coefficients using eq.2.22 and 2.23, would be for the fast mode $\xi \sim 9$ nm and for the slow $\xi \sim 70$ nm.

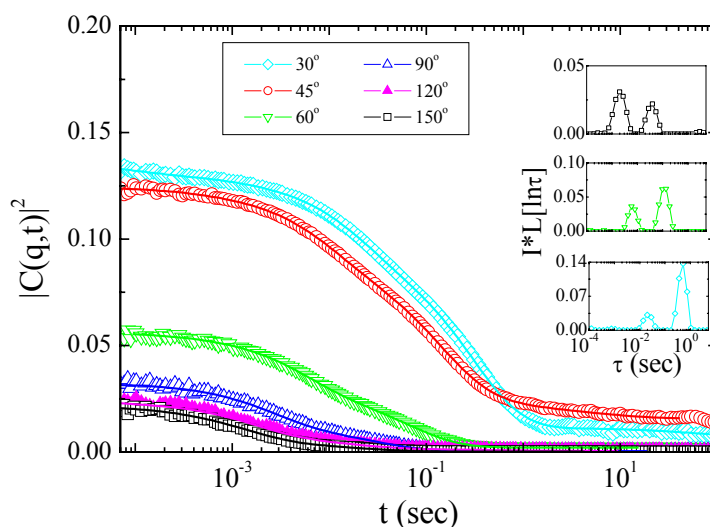


Figure 3.4 Autocorrelation functions of the scattered intensity for different scattering angles of 1wt% I₂S#1 in PI, in 72wt% total polymer concentration. Lines are the fits of Contin. In the inset, the distributions of the relaxation times are shown multiplied by the total scattered intensity, normalized with that of toluene.

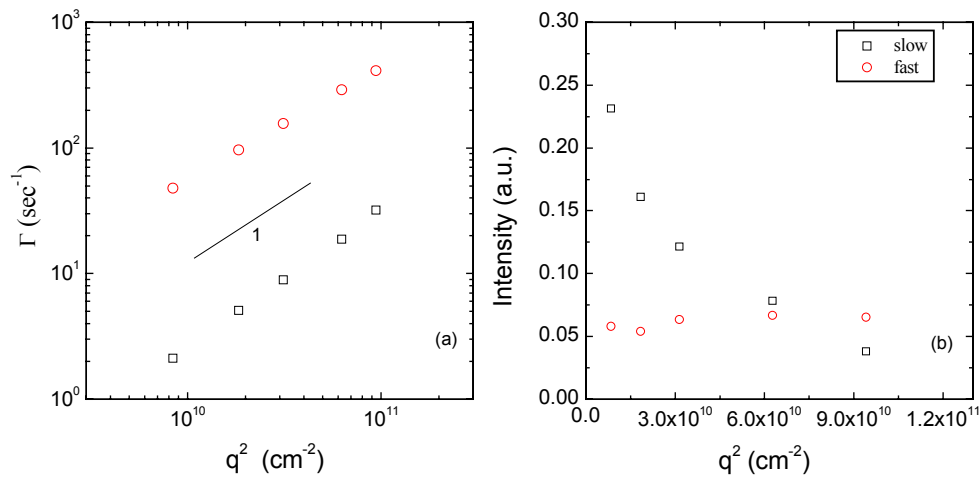


Figure 3.5 Wavevector dependence of (a) the relaxation rate and (b) the scattered intensity for the two processes of 1wt% I₂S#1 in PI, in 72wt% total polymer concentration.

Summarizing the concentration dependence for the specific sample, Figures 3.6 compares the autocorrelation functions at 90° scattering angle, for different polymer concentrations. It is clear that for all concentrations the autocorrelation functions have very low contrast and the Contin analysis reveals two relaxation processes. The inset shows the respective distribution of relaxation times.

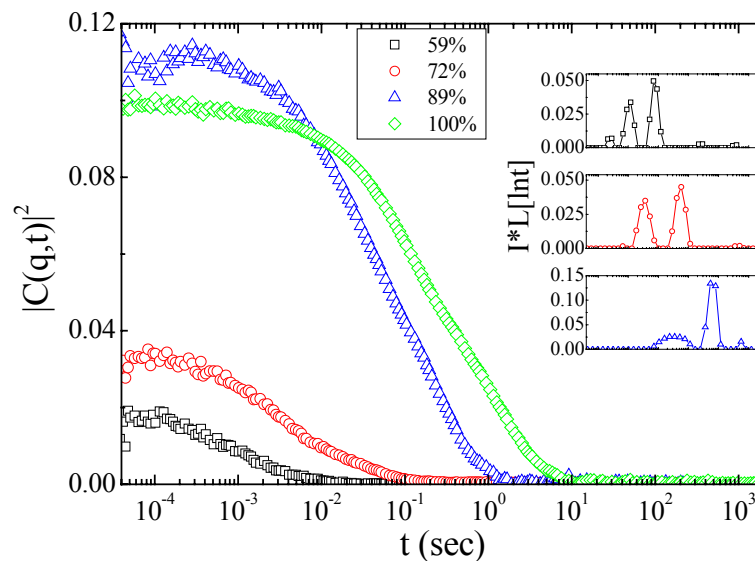


Figure 3.6 Intensity autocorrelation functions for 1wt% I₂S#1 in PI for 90° scattering angle and different polymer concentrations.

Moreover, Figure 3.7 shows the concentration dependence of the intensity and the diffusion coefficient of the two processes. We observe that the increase of the intensity (Figure 3.7(a)) of the fast process is proportional to the concentration, at the specific angle, whereas the increase of the intensity of the slow process is more than that of the respective total polymer concentration. We also observe that for both processes, the diffusion coefficient decreases as we go to higher weight percents of polymer in the sample, a fact that can be attributed to the increase of the viscosity. Consequently the processes become slower.

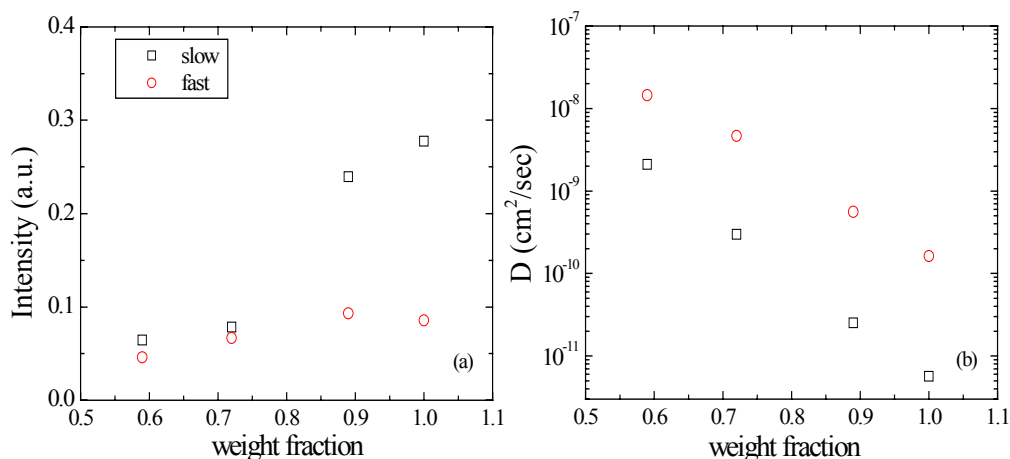


Figure 3.7 Concentration dependence of (a) the scattered intensity (b) the diffusion coefficient for 1wt% I₂S#1 in PI for 90° scattering angle.

We can conclude that even for I₂S#1 concentration 1wt% in PI the situation resembles that of 0.5wt%. Two relaxation processes exist that are diffusive ($\Gamma = D \cdot q^2$), have very low intensities in all measurements and certainly do not indicate any micelle formation.

3.1.3 I₂S#1 2wt% in PI

Since, from the results, concerning the 0.5wt% and 1wt% copolymer in PI, we assumed that no micelles were formed, we attempted to increase the copolymer concentration even further, i.e. to have 2wt% of I₂S#1 in the matrix. The first

measurement that has been performed was again for the lower total polymer concentration, specifically 46wt% in toluene. In Figure 3.8 the autocorrelation functions of the scattered intensity for different scattering angles are shown.

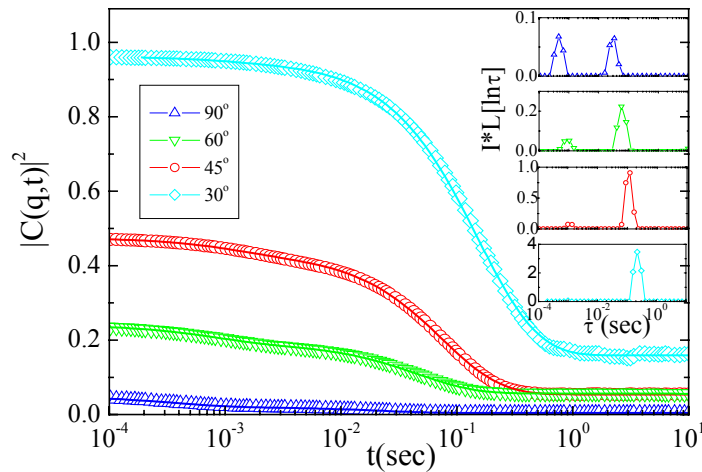


Figure 3.8 Autocorrelation functions of the scattered intensity for different angles of 2wt% I₂S#1 in PI and 46wt% total polymer concentration. The lines are the fits with Contin. In the insets, the distributions of the relaxation times are shown multiplied by the total scattered intensity, normalized with that of toluene.

From Figure 3.8, we observe that, in all angles, the autocorrelation consist of multiple relaxation processes. This is obvious not only from their shape (lines are fits with superposition of exponential functions), but also from the distributions of the relaxation times (insets). From the area under the peaks we calculate the intensity of the processes, whereas from the position of the peaks, the relaxation time. We observe that for both processes the relaxation time slows down as the scattering angle decreases. For the fast process the intensity is almost q -independent. Nevertheless, the slow process has an increasing intensity from ($\sim 2 \cdot 10^{-2} - 4$ a.u.) (note the different scale in the y-axis of the inset). These characteristics are shown in Figure 3.9.

Again, from the relaxation time of the fast process, we assume that it corresponds to the diffusion of the chains in PI matrix and the other process is the so-called, slow mode.^(2,3,4)

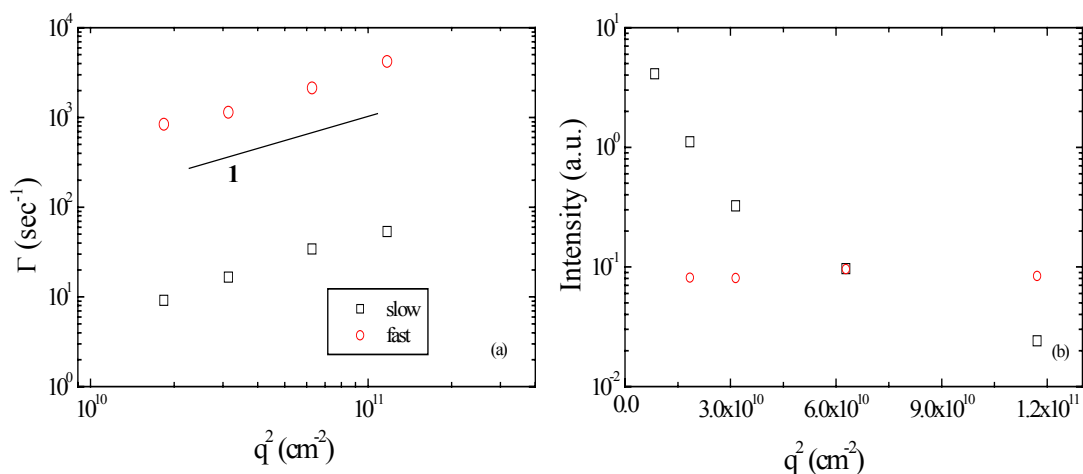


Figure 3.9 Wavevector dependence of (a) the relaxation rate (in a log-log representation) and (b) the scattered intensity for the 2wt% I₂S#1 in PI, in 49wt% toluene solution.

The behavior of the sample does not change significantly if the polymer concentrations are increased. In Figure 3.10 the autocorrelation functions of the scattered intensity are shown for different scattering angles of 2wt% I₂S#1 in PI, in the bulk state.

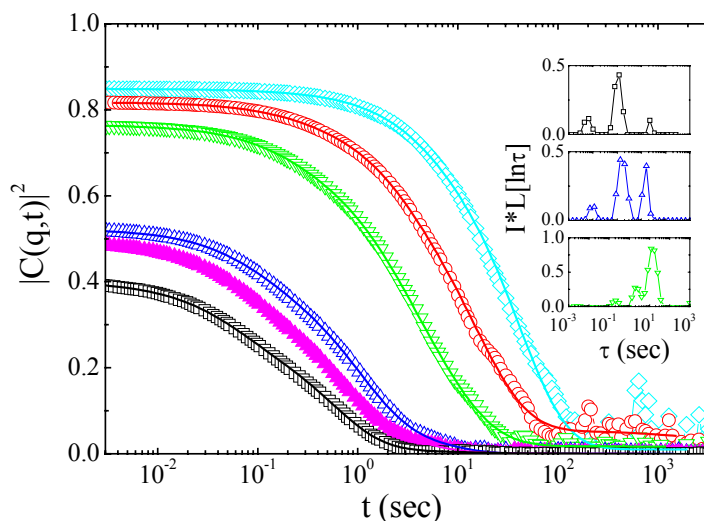


Figure 3.10 Autocorrelation functions of the scattered intensity for angles (—□—) 150°, (—▲—) 120°, (—△—) 90°, (—▽—) 60°, (—○—) 45°, (—◇—) 30° of PI with 2wt% I₂S#1 copolymer, in the bulk. In the insets, the distributions of the relaxation times are shown multiplied by the total scattered intensity, normalized with the appropriate intensity of toluene.

For this concentration, in all angles, the autocorrelation functions are quite broad, so there are more than one relaxation processes, as it is obvious also from the distribution of the relaxation times that derives from the CONTIN analysis (insets). We should focus on the fact that all processes have intensities between 0.1-15 a.u. (Figure 3.11(a)) and are diffusive, since the relaxation rate is of the form: $\Gamma \propto q^2$ (Figure 3.11 (b)). Especially, the intensity of the slow process shows a q -dependence.

If we compare the diffusion coefficients (Figure 3.11(b)) with that of former works of the same copolymer in solution⁽¹⁾ and take into account the difference on the viscosity of the samples, we can assume that that fast process corresponds to the self-diffusion of the chains. Moreover, the slow process has been associated with the “long range density fluctuations”^(2,3,4).

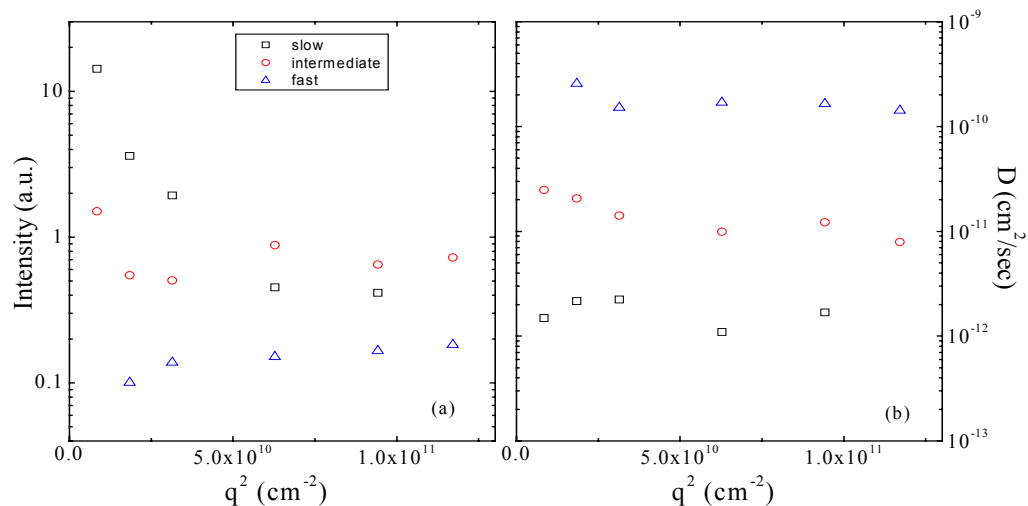


Figure 3.11 Wavevector dependence of (a) the scattered intensity (b) the diffusion coefficient for the various processes of 2wt% I₂S#1 copolymer in PI, in bulk.

Concluding for I₂S#1 block copolymer in homopolymer PI matrix, in all copolymer concentrations (0.5, 1 and 2wt%), the information that Dynamic Light Scattering provides about the dynamics of the polymer chains, led us to the conclusion that this copolymer does not form micelles, at least not for this copolymer concentration, which is attributed to its very small PS block.

3.2 I₂S#5 in PI

After the study of the copolymer/homopolymer mixture that contains the graft copolymer I₂S#1, which has a short polystyrene block ($f_{PS}=0.09$) and which indicated no micelle formation, a similar study but with I₂S#5 which has $f_{PS}=0.64$, in PI matrix, was followed. A series of measurements were carried out for I₂S#5 at 0.5, 1 and 2wt% in PI, for several total polymer concentrations in toluene from 50wt% up to the bulk. The results for these samples are presented in the following sections.

3.2.1 I₂S#5 2wt% in PI

Primarily a solution of 52wt% total polymer concentration in toluene that comprises of 2wt% I₂S#5 in PI was studied. The autocorrelation functions of the scattered intensity for different scattering angles of the specific sample are shown in Figure 3.12.

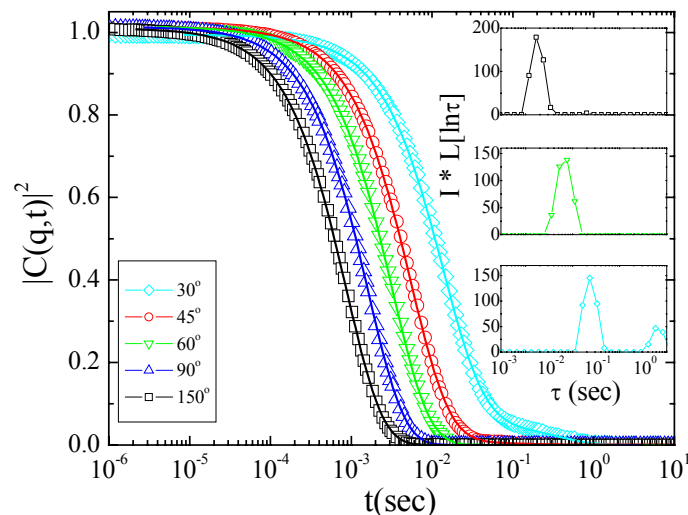


Figure 3.12 Autocorrelation functions of the scattered intensity for the 2wt% I₂S#5 copolymer in PI and for 52wt% polymer concentration. In the insets, the distributions of the relaxation times are shown multiplied by the total scattered intensity, normalized to that of toluene.

It is clear, in contrast to I₂S#1, that in all angles that the autocorrelation functions possess full contrast and relax as a single exponential. This is obvious not only from their shape but also from the distributions of the relaxation times (insets). As the scattering angle decreases, the relaxation time of the process becomes slower, whereas the intensity is q -independent. These characteristics are shown as a function of the scattering wavevector in Figure 3.13, where indeed the scattered intensity is constant and the relaxation rate is of the form $\Gamma \propto q^2$.

This behavior is entirely different from the one observed for the previous system studied (I₂S#1 / PI). Note also the very high scattered intensity. We can attribute this difference in the formation of micelles in the homopolymer matrix, with the PS block of the copolymer forming the core and the PI blocks being mixed with the PI of the matrix.

Figure 3.13 indicates that the dynamics follows a $\Gamma \propto q^2$ dependence showing that the micelles diffuse in the homopolymer matrix. From the diffusion coefficient, D , of this motion we can calculate the hydrodynamic size of the micelles.

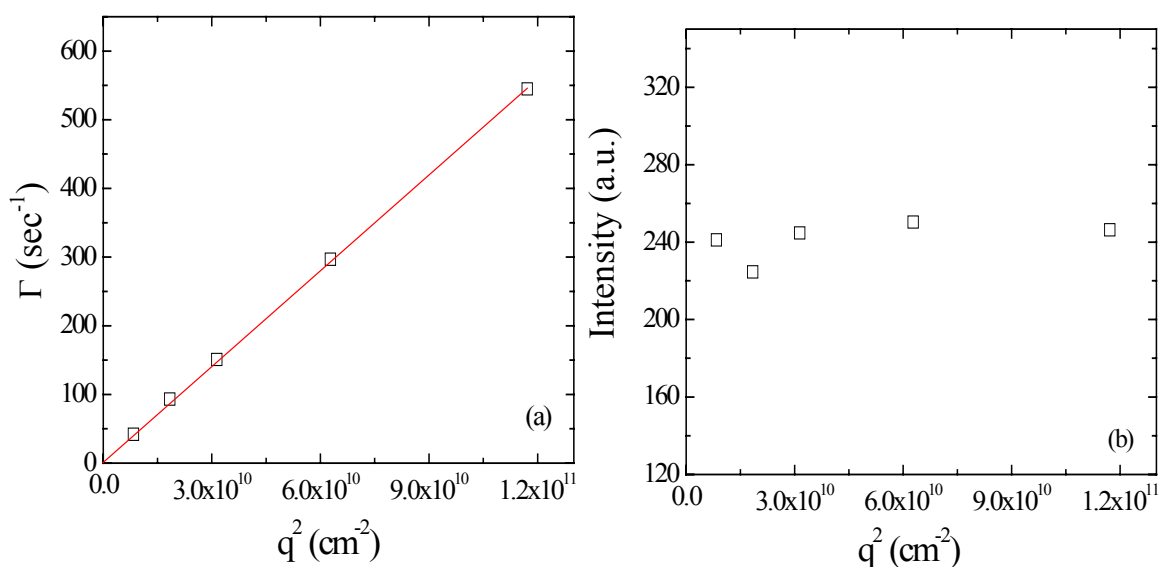


Figure 3.13 Wavevector dependence of (a) the relaxation rate and (b) the scattered intensity of 2wt% I₂S#5 copolymer in PI, in 52wt% total polymer concentration.

The linear fit at the relaxation rate (Figure 3.13(a)) is of the form $\Gamma = 4,83 \times 10^{-9} q^2$

where the slope of the fit corresponds to the diffusion coefficient. Consequently $D=4,83 \times 10^{-9} \text{ cm}^2/\text{sec}$ and from the relation

$$R_H = \frac{kT}{6\pi\eta D} \quad (3.1)$$

using the appropriate value for the viscosity $\eta=0,014 \text{ Pa s}$ that has been measured and the results will be presented analytically in next section, we get a value of $R_H = 33 \text{ nm}$.

The next step, after the study of the I₂S#5/PI in 52wt% in toluene, was the increase of the concentration gradually up to the bulk. The comparison of the autocorrelation functions at 90° scattering angle in different concentrations is shown in Figure 3.14, where we can observe that in all concentrations a single exponential relaxation appears, which defines the existence of a single relaxation process. This process is diffusive, since the relaxation rate for all concentrations, is proportional to the square of the wavevector ($\Gamma \propto q^2$) (Figure 3.15(a)) and has very high intensity that increases with concentration (Figure 3.15(b)). Also, as the total polymer concentration increases, the intensity of the relaxation process increases but the hydrodynamic radius decreases.

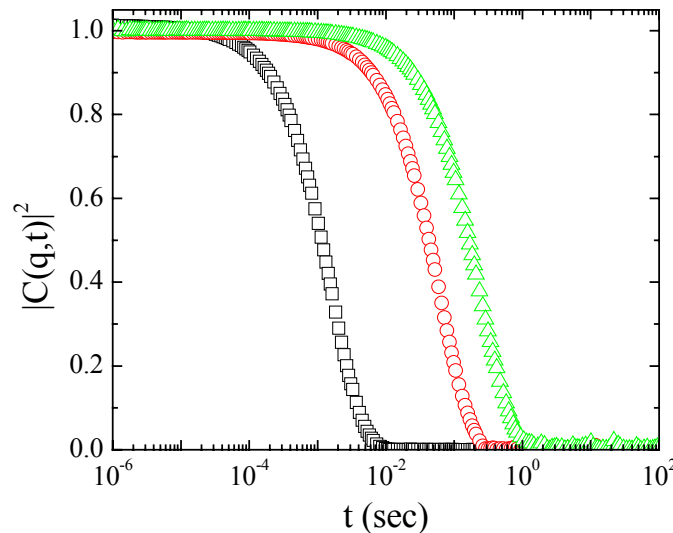


Figure 3.14 Autocorrelation functions of I₂S#5 in concentrations (□) 52wt%, (○) 90wt% and (△) 100wt% at 90° scattering angle.

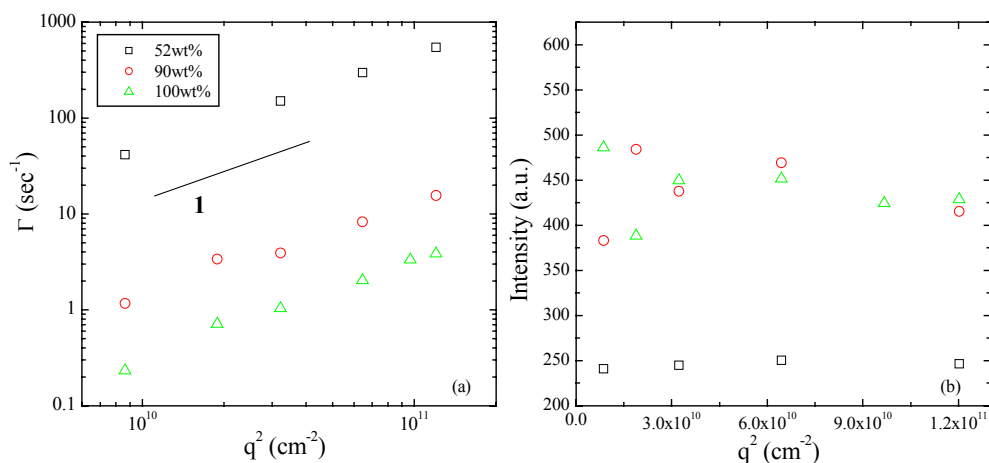


Figure 3.15 Dependence from the scattering vector of: (a) the relaxation rate and (b) the scattered intensity of the process, for the various concentrations of I₂S#5/PI in toluene.

From the relaxation rate (Figure 3.15(a)) we can calculate the diffusion coefficient for the different concentrations and we examine the change in the hydrodynamic size of the micelles. For these calculations the concentration dependence of the viscosity that will be presented analytically in section B of this chapter has been taken into account. The results of these calculations are shown in Table 3.1.

Table 3.1

Concentration in toluene	52wt%	90wt%	100wt%
η (Pa s)	0,016	0,548	3,037
R_H (nm)	33	31	22

From these results we can conclude that as the concentration in toluene is increased, the micelles obtain smaller size and become more compact. That means that the solvent, when present, penetrates in the micelle's core and makes it bigger.

3.2.2 I₂S#5 1wt% in PI

Since at 2wt% copolymer concentration there was micelle formation in all the different solutions of I₂S#5 in PI, we decided to decrease the copolymer concentration in order to check if there is any change in the sample's behavior. So the copolymer

concentration was decreased at 1wt% and again the first measurement was performed for 57wt% in toluene. The autocorrelation functions for different scattering angles are shown in Figure 3.16. It is clear that the behavior resembles the one of the 2wt% I₂S#5 in PI since there is one relaxation process that becomes slower as the scattering angle decreases.

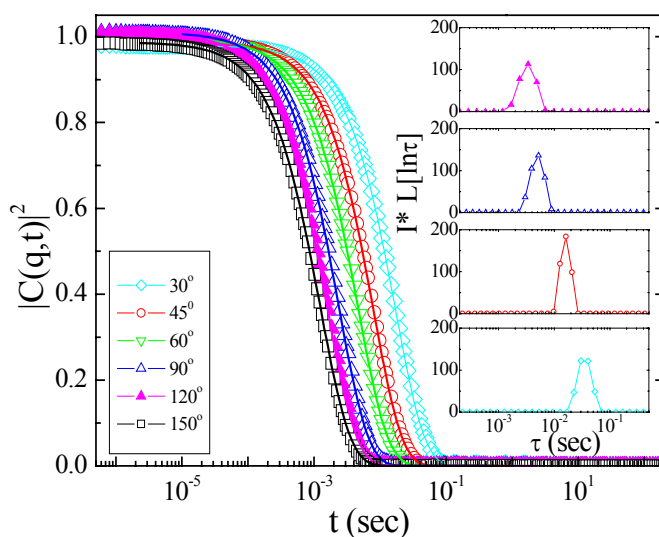


Figure 3.16 Autocorrelation functions of the scattered intensity for different angles of 1wt% I₂S#5 in PI, in concentration 57wt% in toluene. The lines are fits of the Contin analysis. In the insets, the distributions of the relaxation times are shown multiplied by the total scattered intensity, normalized to that of toluene.

Moreover, this process is diffusive and has very high intensity, about 180 a.u., which is q -independent (as it is shown in Figure 3.17(b)). The diffusion coefficient can be calculated from the slope of the relaxation rate (Figure 3.17(a)) and is equal to $D = 3.24 \times 10^{-9} \text{ cm}^2/\text{sec}$. This value leads to a hydrodynamic radius for the micelles of $R_H = 31 \text{ nm}$.

The value of the hydrodynamic radius has been calculated using the appropriate value of the viscosity for this concentration and temperature that has been measured for the specific sample and will be presented in following section.

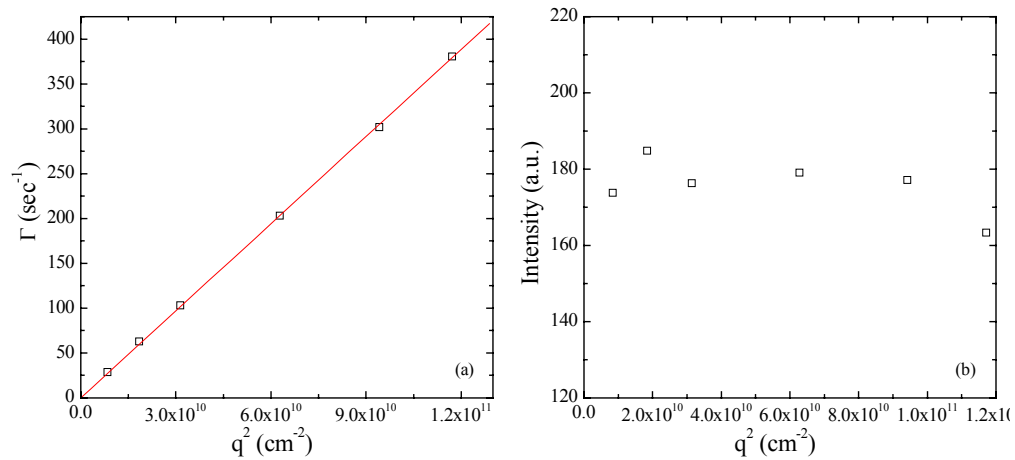


Figure 3.17 Scattering wavevector dependence of: (a) the relaxation rate and (b) the scattered intensity of the process in 1wt% I₂S#5 in PI, in 57wt% total polymer concentration.

The dynamics of I₂S#5 1wt% in PI has been studied extensively for different concentrations up to the bulk state. The results from these measurements are summarized in Figure 3.18, where the autocorrelation functions are presented, and in Figure 3.19, where the intensity and the diffusion coefficient of the process are shown for all total polymer concentrations.

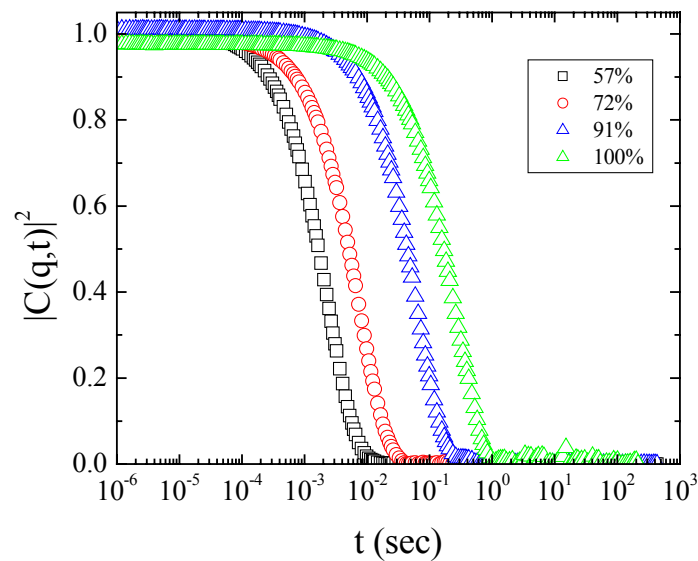


Figure 3.18 Intensity autocorrelation functions of 1wt% I₂S#5 in PI, for different concentrations at 90° scattering angle.

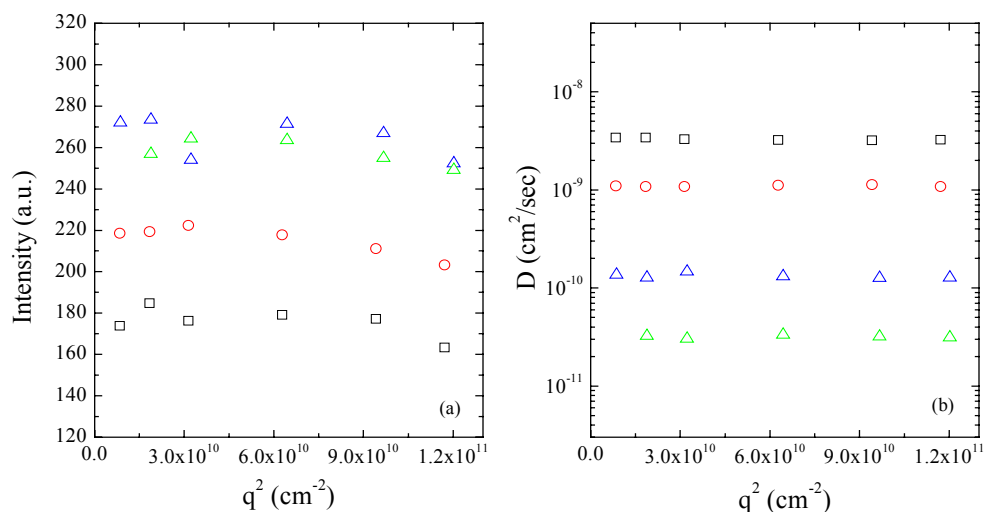


Figure 3.19 Scattering wavevector dependence of: (a) the scattered intensity and (b) the diffusion coefficient of the relaxation process of 1wt% I₂S#5 in PI, for total polymer concentrations (□) 57wt%, (○) 72wt% (△) 91wt% and (▽) 100wt% in toluene.

From the correlation functions is apparent that there is only one relaxation process that slows down as the concentration increases. This process has an increasing intensity that is q -independent and a decreasing diffusion coefficient as the solvent (here toluene) evaporates. The results for the hydrodynamic radii of the micelles in all concentrations are shown in Table 3.2. In the same table the intensity of this process is also shown.

Table 3.2

Concentration in toluene (wt%)	Intensity (a.u.)	η (Pa s)	R_H (nm)
57	175	0,023	31
72	215	0,065	30
91	270	0,619	29
100	272	3,037	22

Examining the above results we can conclude that for this copolymer concentration, as well as for the 2wt%, micelles exist that become more compact as the amount of the solvent decreases. So the presence of the toluene influences the size of the micelles probably because it is spread not only in the “hair” but also in their “core” of the micelles.

As a final point, from the comparison of the hydrodynamic radius for this copolymer concentration with that for 2wt% in PI, we observe that in both cases the micelles have the same size in the bulk state.

3.2.4 I₂S#5 0.5% in PI

Following the results of I₂S#5/PI at 2wt% and 1wt% we attempted to dilute even more the copolymer, so a mixture was prepared with an even lower copolymer concentration in PI that is 0.5wt%. Figure 3.20 shows the autocorrelation functions of 56wt% polymer in toluene, for different scattering angles.

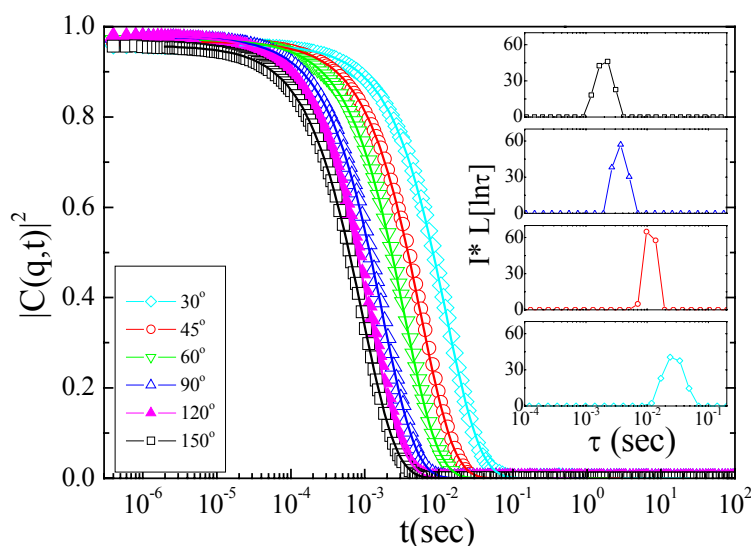


Figure 3.20 Autocorrelation functions of the scattered intensity for different angles of 0.5wt% I₂S#5 in PI, in 56wt% total polymer concentration. The lines are from the Contin analysis. In the insets, the distributions of the relaxation times are shown multiplied by the total scattered intensity, normalized to that of toluene.

In all angles, the autocorrelation functions have full contrast and correspond, as for 1 and 2wt%, to one relaxation process. This is apparent both from the shape of the functions and the distribution of the relaxation time (insets). Moreover, the process has high intensity (Figure 3.21(b)) that indicates the formation of micelles in the sample.

From the relaxation rate (Figure 3.21(a)) the diffusion coefficient can be calculated resulting in a hydrodynamic radius of $R_H = 34nm$.

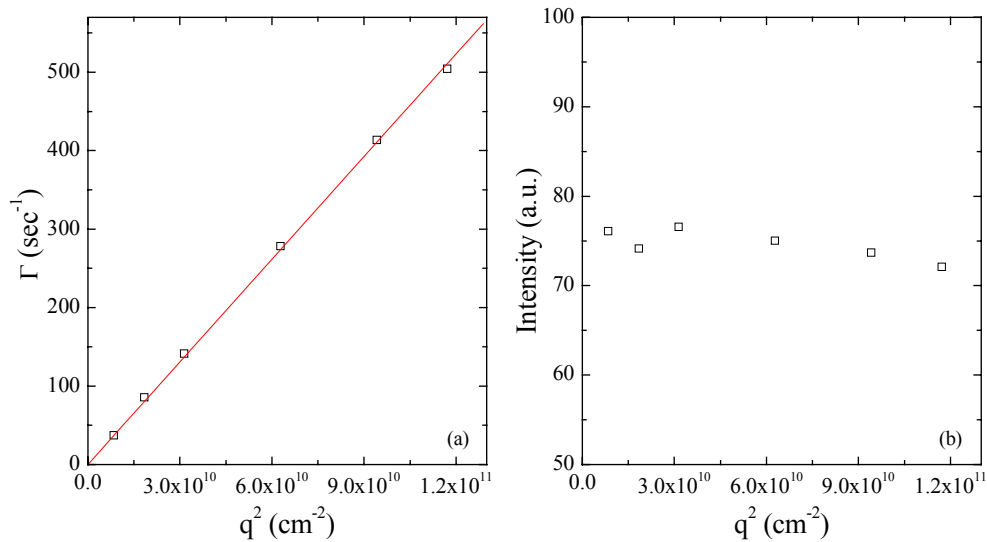


Figure 3.21 Scattering wavevector dependence of: (a) the relaxation rate and (b) the scattered intensity of the process for 0.5wt% I₂S#5 in PI, for 56wt% total polymer concentration.

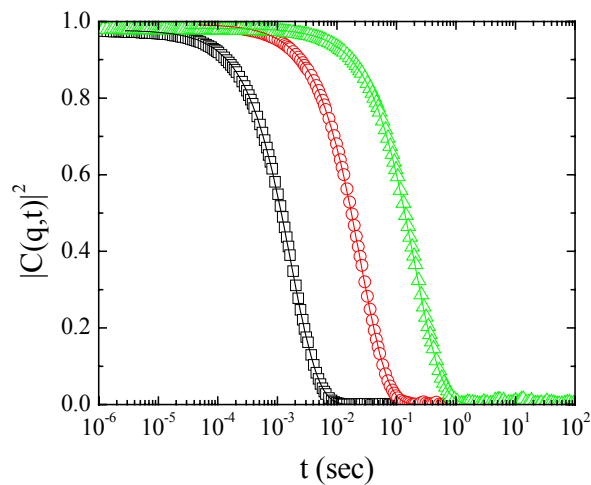


Figure 3.22 Autocorrelation functions of 0.5wt% I₂S#5 in PI, for total polymer concentrations (□) 56wt%, (○) 85wt% (△) 100wt% at 90° scattering angle. The lines are the fits of the CONTIN analysis.

To conclude with, we performed a series of measurements for different concentrations of the polymer. From these results we observe that for all concentrations the autocorrelation functions (Figure 3.22) are single exponential with full contrast and move to longer time as the concentration increases.

It seems that micelles are formed in all concentrations, we assume that the high values of the intensity is an indication of their existence (Figure 3.23 inset). From Figure 3.23 we observe that as the concentration increases the diffusion coefficient decreases whereas the intensity of the process increases. Again, as in 1wt% and 2wt%, the size of the micelles becomes smaller indicating that they become more compact and this affects the scattered intensity probably since there is change in the refractive index.

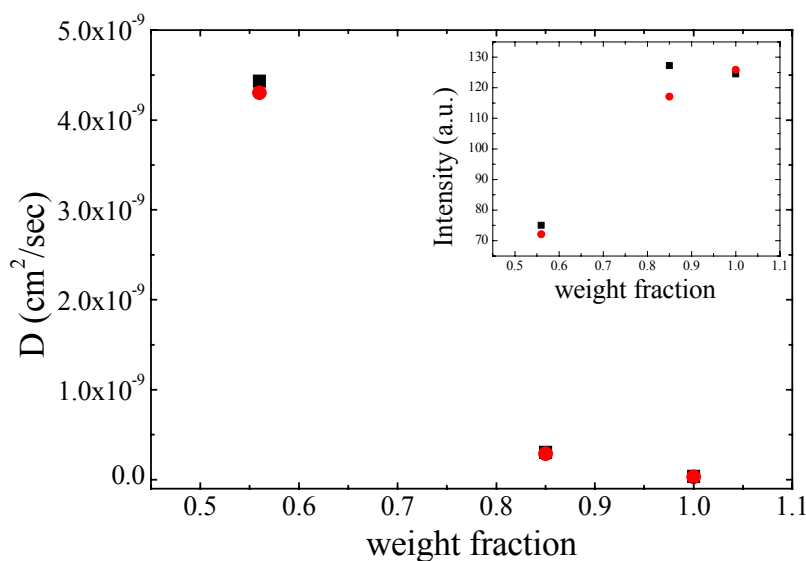


Figure 3.23 Diffusion coefficient of 0.5wt% I₂S#5 in PI as a function of the total polymer concentration for (■) 90° and (●) 150° scattering angles. In the inset the concentration dependence of the intensity is shown for scattering angles (■) 90° and (●) 150°.

Lastly, if we compare the results for the different copolymer concentrations of I₂S#5 in PI (Figure 3.24), we observe an increase of the intensity going from 0.5wt% to

2wt%. This may be evidence that the number of micelles increases in the sample with the copolymer concentration which is less for 0.5wt% than for 2wt%. It should also be emphasized that the diffusion coefficient doesn't change with the increase of copolymer concentration, so the micelles that are formed are almost of the same size, $R_H \sim 22-24\text{nm}$.

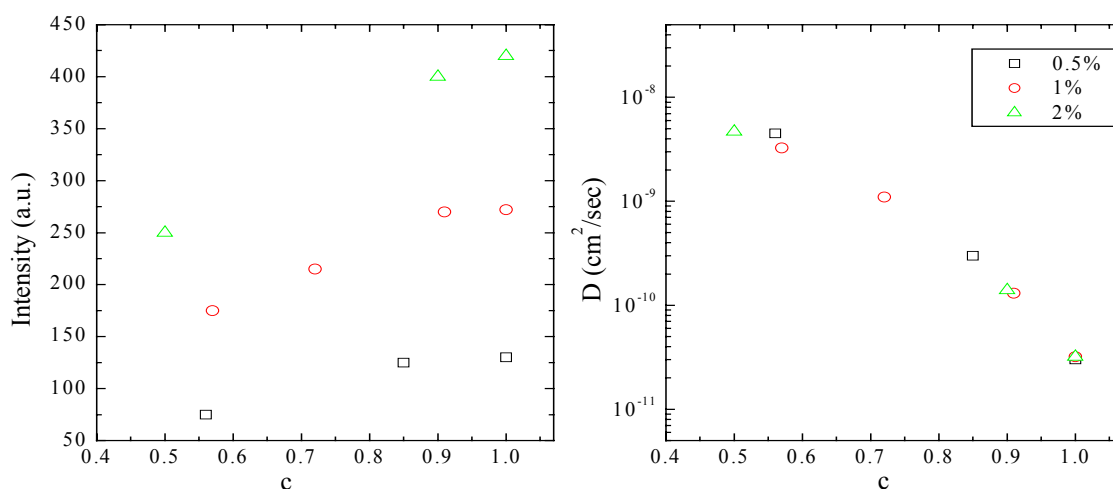


Figure 3.24 Total polymer concentration dependence of: (a) the intensity and (b) the diffusion coefficient of the process for (□) 0.5, (○) 1 and (△) 2wt% of I₂S#5 graft copolymer in the homopolymer PI matrix.

3.3 I₂S#3 1wt% in PI

The results from the investigation of the previous copolymer/homopolymer mixtures that showed existence of micelles in all concentrations of I₂S#5 ($f_{PS}=0.64$) in PI and no micelles in all concentrations of I₂S#1 ($f_{PS}=0.09$) in PI, created the interest for the study of one mixture with a graft copolymer that has an intermediate composition in comparison with the other two graft copolymers. Therefore the last graft copolymer that has been studied is I₂S#3 that consists of 35wt%PS. A series of measurements were carried out for this copolymer at concentration 1wt% in PI.

As for most samples, the initial studied concentration was 50wt%. Figure 3.25 shows the autocorrelation functions of the scattered intensity of I₂S#3 1wt% in PI, in this total polymer concentration, for different scattering angles. Their shape is similar with that of I₂S#1 graft copolymer in PI, specifically they are broad, with low contrast and correspond to multiple processes. This is obvious also from the distributions of the

relaxation times (inset). Specifically, there are two relaxation processes that shift to slower relaxation time as the scattering angle decreases.

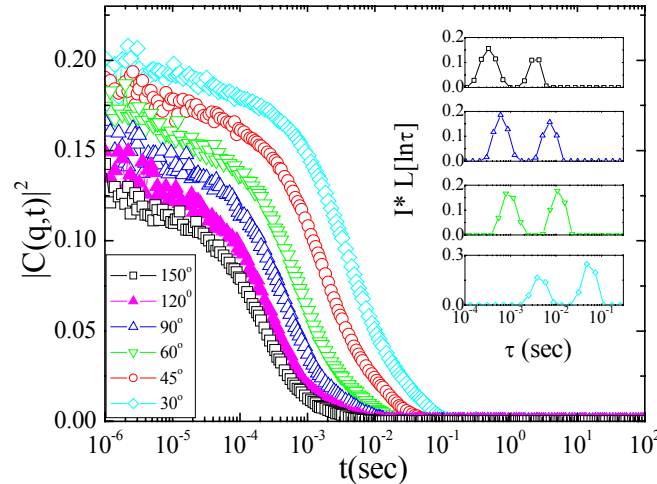


Figure 3.25 Autocorrelation functions of the scattered intensity for different scattering angles of 1wt% I₂S#3 in PI, in 50wt% concentration in toluene. The lines are fits with superposition of exponentials. In the inset, the distributions of the relaxation times are shown multiplied by the total scattered intensity, normalized with that of toluene.

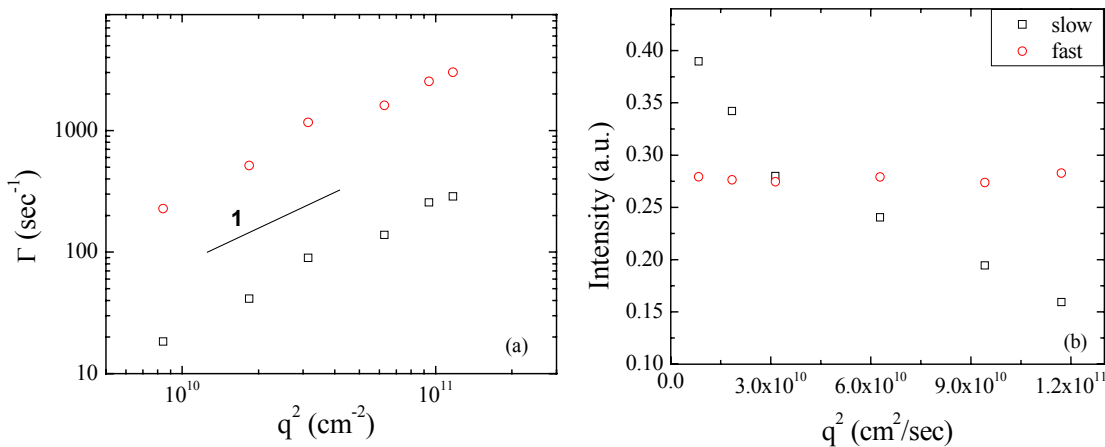


Figure 3.26 Dependence from the scattering wavevector of: (a) the relaxation rate of the process and (b) the scattered intensity.

Moreover, the results for the intensity and the relaxation rate are shown in Figure 3.26. The fast process has a low and q -independent intensity, while the slow shows q -

dependence and decreases as the wavevector increases. Nevertheless, they are both diffusive since the relaxation rate is of the form $\Gamma \propto q^2$, shown in Figure 3.26(a).

As a next step, the polymer concentration was increased in 70wt% in toluene. The results of the measurements in this concentration are shown in Figure 3.27 and 3.28, where it is clear that the behavior of this sample drastically changes and resembles the one of I₂S#5. The autocorrelation functions are now single exponential, with high contrast and correspond to one single process. This is obvious also from the distribution of the relaxation time (inset). This process slows down at small angles and but has constant intensity of about 20a.u. that is extremely higher than the intensity at 50wt%. Since the behavior in this concentration is entirely different from the one in 50wt% total polymer concentration, we can assume that there is micelle formation.

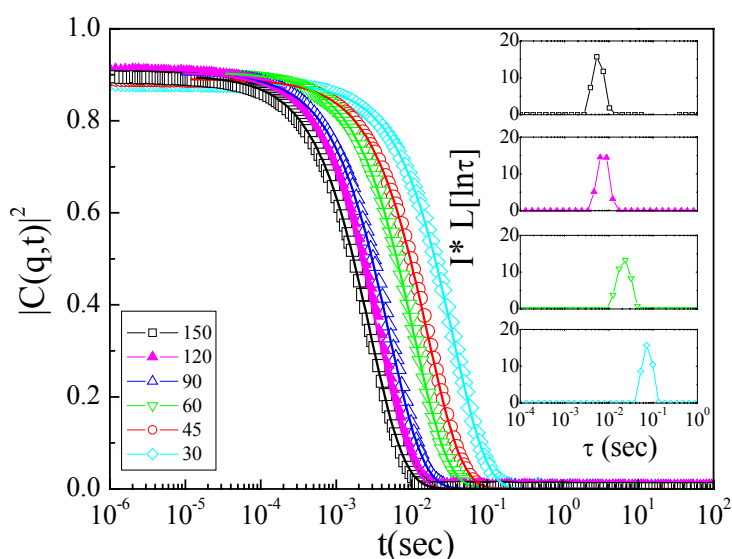


Figure 3.27 Autocorrelation functions of the scattered intensity for different scattering angles of 1wt% I₂S#3 in PI, in 70wt% total polymer concentration. The lines are fits with single exponentials. In the inset, the distributions of the relaxation times are shown multiplied by the total scattered intensity, normalized with that of toluene.

Figure 3.28 indicates that the dynamics of these micelles follow a $\Gamma \propto q^2$ dependence showing that they diffuse in the homopolymer matrix. From the

diffusion coefficient of this motion, $D = 1.5 \cdot 10^{-9} \text{ cm}^2/\text{sec}$ and the respective value of the viscosity for this polymer concentration, we can calculate the hydrodynamic size of the micelles that is $R_H = 27 \text{ nm}$.

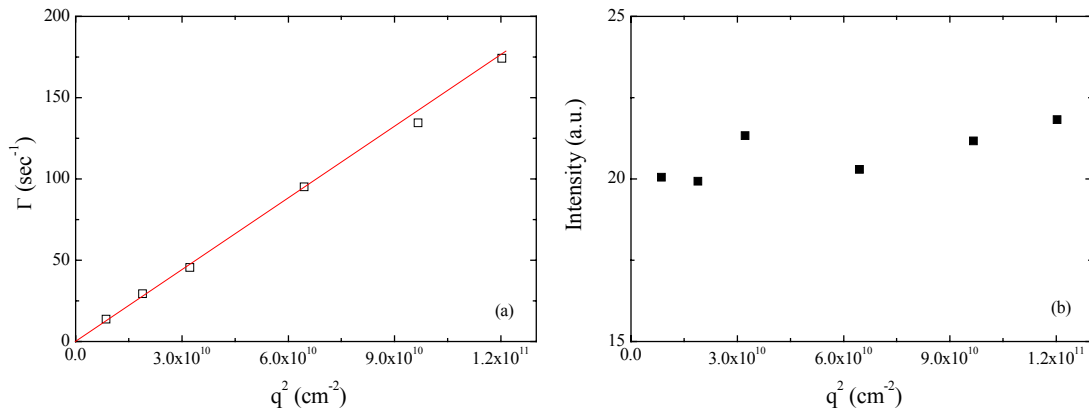


Figure 3.28 Wavevector dependence of (a) the relaxation rate and (b) the scattered intensity of the process, for 1wt% I₂S#3 in PI, in 70wt% total polymer concentration.

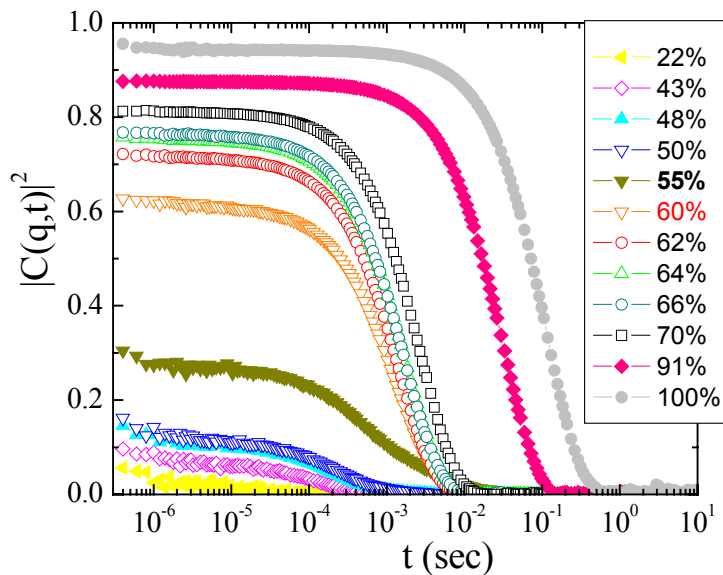


Figure 3.29 Intensity autocorrelation functions of 1wt% I₂S#3 in PI, for different total polymer concentrations at 150° scattering angle.

Since, there is obviously a drastic change in the behavior of I₂S#3 between 50 and 70wt%, we decided to perform a series of measurements at a number of different

concentrations from 22wt% till the bulk state, in order to scan in detail the whole concentration regime and define the concentration at which we have the micelle formation. The results are summarized in Figure 3.29 where the concentration dependence of the intensity autocorrelation function for scattering angle $\theta=150^\circ$ is shown. In this Figure we can observe the change of the shape as the total polymer concentration increases. It starts at 55wt% and becomes more obvious above 60wt%, where the autocorrelation function becomes single exponential and has higher contrast. Additionally the total scattered intensity shown in Figure 3.30, increases linearly with the concentration for low concentrations, but shows a sharp change above 60wt%, a result that indicates the formation of micelles. From this we can estimate that the micelles are formed at concentrations $\sim 55\text{-}68\text{wt}\%$. In the bulk state the size of the micelles is calculated to be $R_H=20\text{nm}$, slightly smaller than the other graft copolymer (I₂S#5) that has been investigated already.

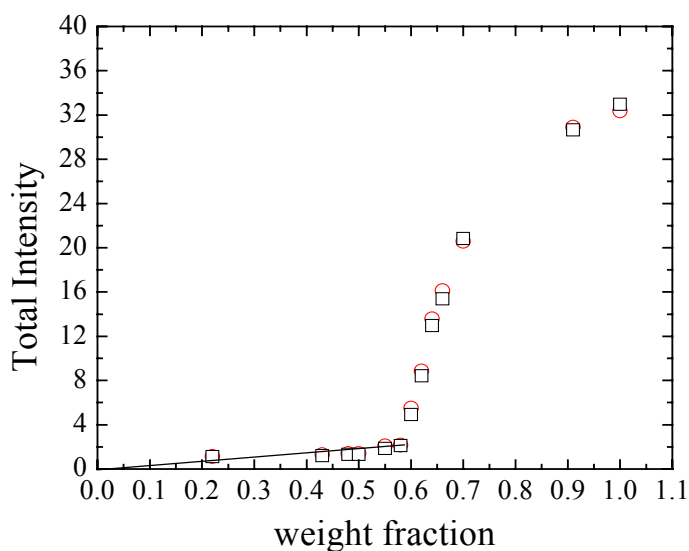


Figure 3.30 Concentration dependence of the total intensity for (○) 90° and (□) 150° scattering angles of 1wt% I₂S#3 in PI.

□ Effect of architecture/Linear copolymer-homopolymer blends

3.4 Linear diblock copolymer PS₃₀PI₇₀

The dependence of micelle formation on the molecular architecture was investigated by using linear diblock copolymers with similar molecular weights and compositions with those of the graft copolymers studied, so far. The linear copolymers used are polystyrene-polyisoprene diblocks with different composition in PS, the one is rich and the other poor in PS. The first linear diblock copolymer used PS₃₀PI₇₀, has similar polystyrene composition with the graft copolymer I₂S#3, namely $f_{PS}=0.29$. Figure 3.31 shows the autocorrelation functions of the scattered intensity of 1wt% PS₃₀PI₇₀, in 35wt% total polymer concentration, for different scattering angles.

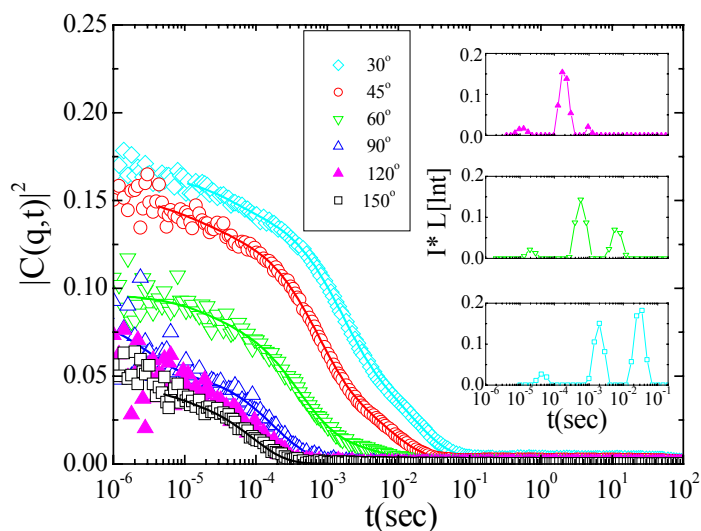


Figure 3.31 Autocorrelation functions of the scattered intensity for different scattering angles of 1wt% PS₃₀PI₇₀ in PI, in 35wt% concentration in toluene. In the inset, the distributions of the relaxation times are shown multiplied by the total scattered intensity, normalized with that of toluene.

In all angles the autocorrelation functions show three relaxation processes, as it is also revealed from the CONTIN analysis (inset). The results for the intensity and the relaxation rate of the processes are shown in Figure 3.32. All processes are diffusive and

have low intensities compared to that observed when micelles were present. The situation resembles the one of I₂S#3 ($f_{PS}=0.32$) in low polymer concentrations.

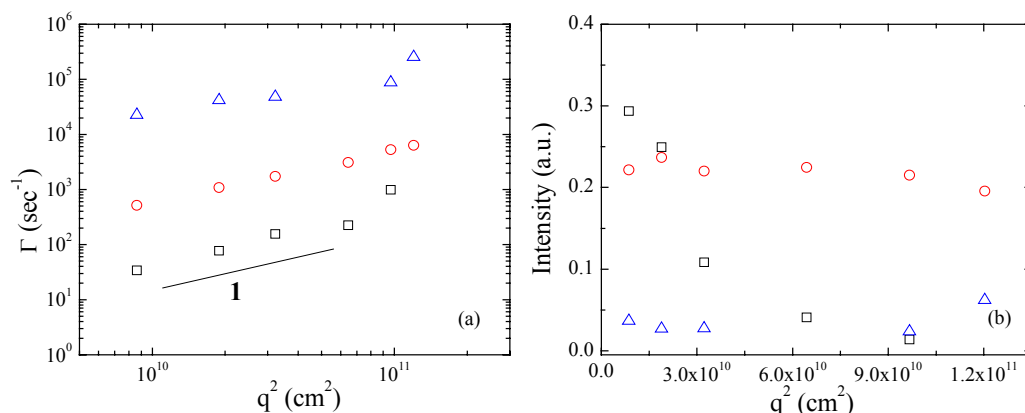


Figure 3.32 Dependence from the scattering vector of: (a) the relaxation rate and (b) the scattered intensity of the processes for 1wt% PS₃₀PI₇₀ in PI, in 35wt% total polymer concentration.

After the study in 35wt% total concentration, the solvent was steadily evaporated from the cell so that higher total polymer concentrations could be achieved. Studying the results for any concentration above 54wt%, we observe a complete change on the behavior of the sample. Specifically, Figure 3.33 shows the intensity autocorrelation functions and the distribution of the relaxation time (inset) for 60wt% total polymer concentration.

In contrast to 35wt%, the decay is single exponential with almost full contrast and reflects to one relaxation process. This process moves to slower relaxation time as the scattering angle decreases (Figure 3.33 inset).

Remarkable is the fact that the intensity of the process (Figure 3.34) is higher than that of the processes in 35wt% almost 100-1000 times. It is clear that there are micelles in this concentration and since the process is diffusive we can estimate the diffusion coefficient and furthermore the hydrodynamic radius, that is $R_H = 43\text{nm}$.

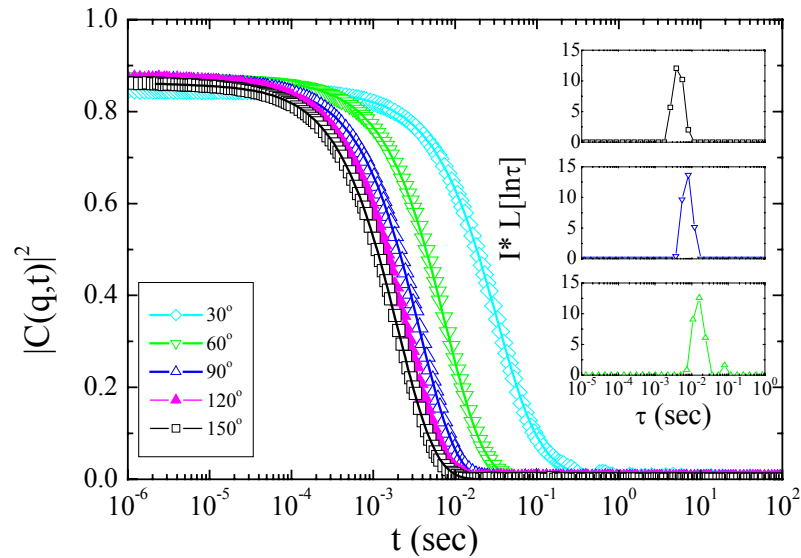


Figure 3.33 Autocorrelation functions of the scattered intensity for different scattering angles of 1wt% PS₃₀PI₇₀ in PI, in 60wt% total polymer concentration. In the inset, the distributions of the relaxation times are shown multiplied by the total scattered intensity, normalized with that of toluene.

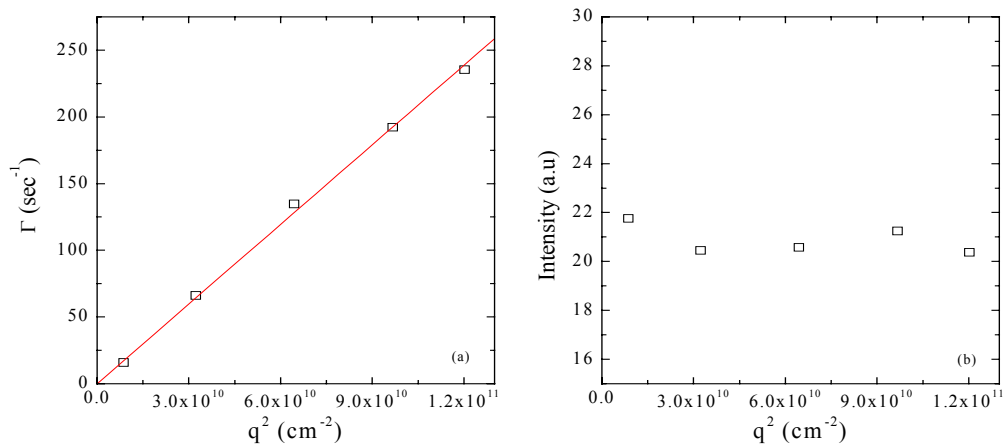


Figure 3.34 Scattering-vector dependence of: (a) the relaxation rate and (b) the scattered intensity of 1wt% PS₃₀PI₇₀ in PI, in 60wt% total polymer concentration.

The results for all the concentrations studied are summarized in Figure 3.35(a) where the autocorrelation correlation functions of this sample are shown at scattering

angle $\theta=150^\circ$. It is clear that the shape of the functions changes to single exponential above 54wt% total polymer concentration. This change in addition with the strong increase of the intensity (Figure 3.35(b)), above this concentration, indicates the micelle formation in the homopolymer matrix, with the PS block of the copolymer forming the core and the PI blocks being mixed with the PI of the matrix.

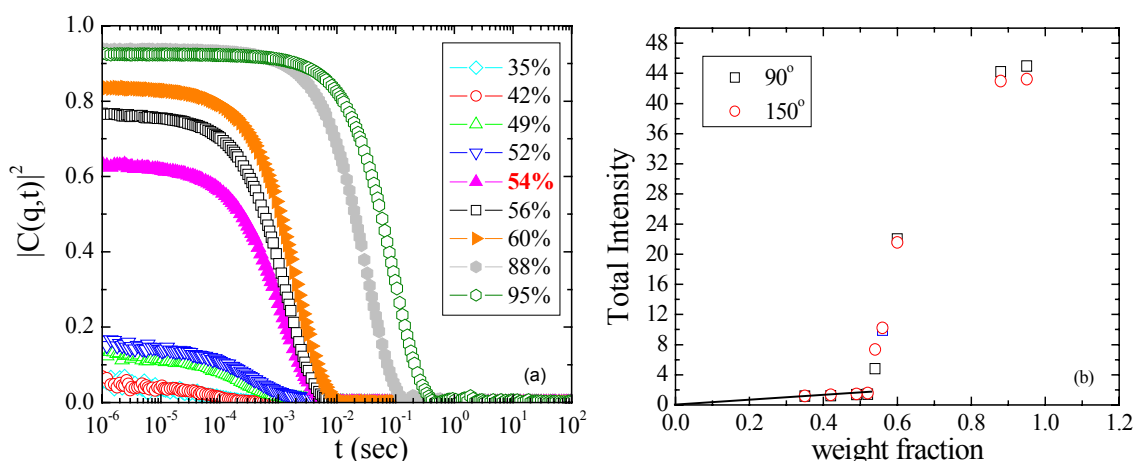


Figure 3.35 (a) Intensity autocorrelation functions of 1wt% PS₃₀PI₇₀ in PI, for total polymer concentrations from (-◇-) 35wt% till (-○-) 95wt% at 150° scattering angle. (b) Concentration dependence of the total intensity for (○) 90° and (□) 150° scattering angles of 1wt% PS₃₀PI₇₀ in PI.

These micelles have a decreasing size as the solvent evaporates which starts from 43nm at 60wt% total polymer concentration and at 95wt% reaches the $R_H=39nm$. The reduction on the size is probably the reason for the increase of the intensity assuming that the micelles become compact.

Closing this section, we can remark that the behavior of this linear diblock copolymer that consists of 32wt% PS is similar with that of the graft copolymer I₂S#3 that consists of 35wt% PS. It has to be noted here, that the concentration at which micelles are formed does not depend strongly on whether the copolymer is linear or graft. This is probably attributed to the fact that in both cases there is one PS block and it is the number of PI blocks that changes from one to two. It would be interesting to examine

whether this concentration would change if a graft copolymer with similar molecular weight and composition was examined but with the chemical form of S_2I . A difference between the two systems may be that the micelles formed by the linear copolymer seem to have a larger size compared to the ones formed by the graft.

3.5 Linear diblock copolymer $PS_{70}PI_{30}$

The architecture effect investigation was completed with the study of PI containing the linear diblock copolymer $PS_{70}PI_{30}$ with $f_{PS}=0.65$ that has similar polystyrene composition with $I_2S\#5$ ($f_{PS}=0.64$). The copolymer concentrations that have been studied are 2wt% and 0.5wt% in PI.

3.5.1 $PS_{70}PI_{30}$ 2wt% in PI

The sample is a mixture of polyisoprene with 2wt% linear copolymer $PS_{70}PI_{30}$ and was initially prepared at 50wt% total polymer concentration in PI. For this concentration the behavior of the sample resembled that of $I_2S\#5$ graft copolymer/homopolymer mixture, with autocorrelation functions with full contrast that correspond to one relaxation process.

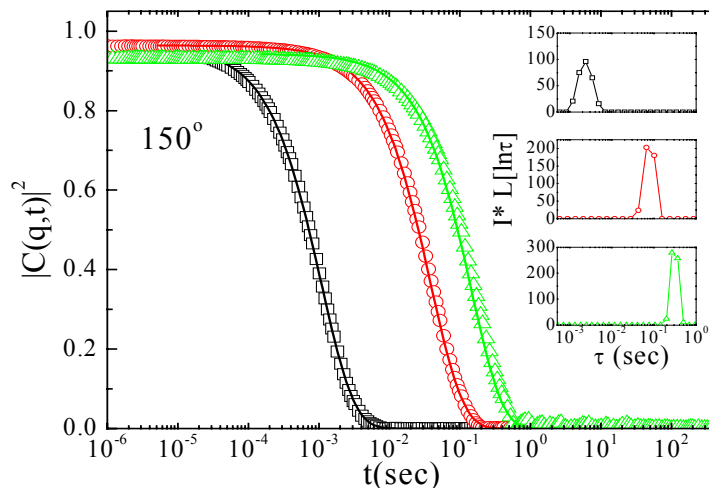


Figure 3.36 Intensity autocorrelation functions of 2wt% $PS_{70}PI_{30}$ in PI, for total polymer concentrations (\square) 50wt%, (\circ) 88wt% and (\triangle) 100wt% at 150° scattering angle. The lines are fits from the Contin analysis.

The next step was to gradually increase the total polymer concentration till the bulk state. Since the sample for all the investigated total polymer concentrations has similar behavior, we have chosen to present the results from the different polymer concentrations together. Figure 3.36 shows the autocorrelation functions for scattering angle $\theta=150^\circ$ of different total polymer concentrations. In all concentrations the decay is single exponential that corresponds to one process, with characteristic relaxation time that is slower at high concentrations. From the analysis of our data we get the intensity of this process (Figure 3.37 (a)) that has very high values and indicates the existence of micelles in the sample. Moreover as the total polymer concentration increases, the intensity of the process rises to even higher values and the diffusion coefficient (Figure 3.37 (b)) decreases.

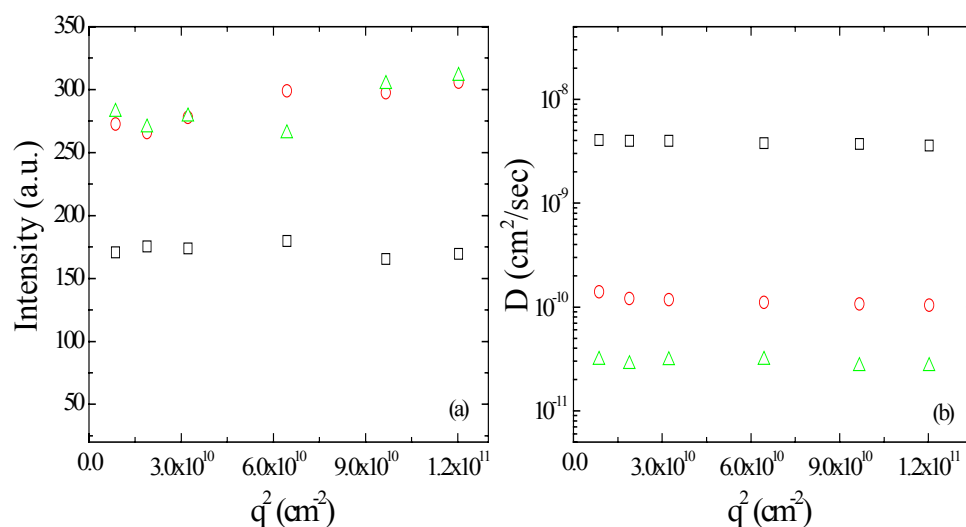


Figure 3.37 Wavevector dependence of (a) the intensity of the process and (b) the diffusion coefficient of 2wt% PS₇₀PI₃₀ in PI for total polymer concentrations (□) 50wt%, (○) 88wt% and (△) 100wt%.

The calculated values for the hydrodynamic radii of the micelles are shown in Table 3.3. For the bulk state, the size of the micelles that are formed from this linear diblock copolymer is bigger than that of the graft copolymer with similar composition. This is something that was also observed for the linear/graft copolymer pair with lower polystyrene content, discussed previously.

Table 3.3.

Concentration in toluene	50wt%	88wt%	100wt%
η (Pa s)	0,014	0,410	3,037
R_H (nm)	41	39	26

3.5.2 PS₇₀PI₃₀ 0.5wt% in PI

The same study at a lower copolymer concentration, namely 0.5wt% in PI was performed in order to dilute the copolymer concentration but found to give similar results. In Figure 3.38 the autocorrelation functions of the scattered intensity are shown at total polymer concentrations that vary from 50wt% to 100wt% in toluene, for scattering angle 90°. It is clear that there is one relaxation process with characteristic relaxation time that changes as the concentration increases.

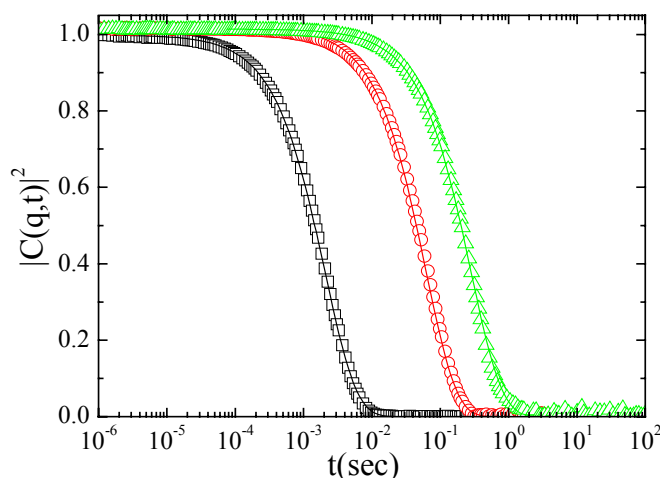


Figure 3.38 Intensity autocorrelation functions of PS₇₀PI₃₀ 0.5wt% in PI in different total polymer concentrations, namely (□) 50wt%, (○) 88wt% and (△) 100wt% in toluene at scattering angle 90°. The lines are fits from the Contin analysis.

A more detailed analysis in each concentration gives us the opportunity to calculate the diffusion coefficients and the intensities of the process (Figure3.39). The

constantly high values of the intensity indicate that there are micelles in the sample. These micelles have a decreasing size as the solvent is evaporating, as well.

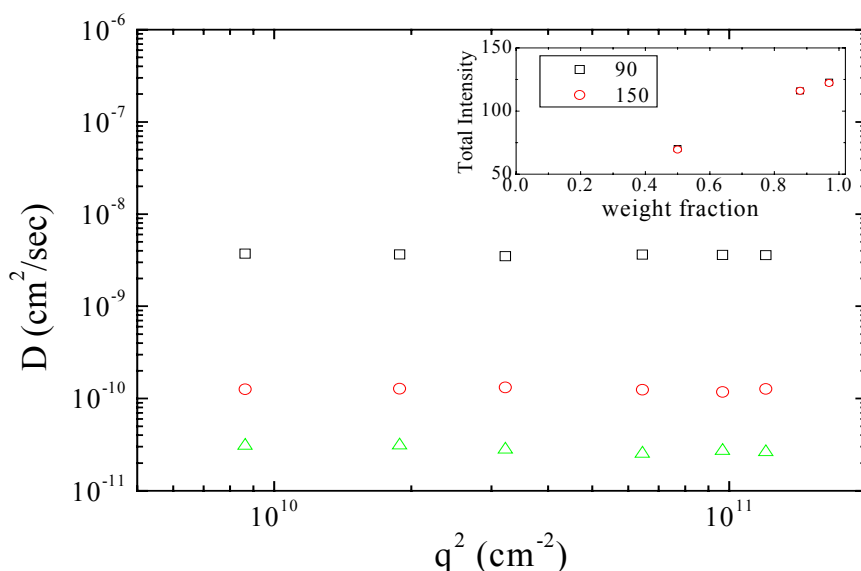


Figure 3.39 Wavevector dependence of the diffusion coefficient for PS₇₀PI₃₀ 0.5wt% in PI for (□) 50wt%, (○) 88wt% and (△) 100wt% total polymer concentrations. In the inset is shown the concentration dependence of the intensity of the process at two different scattering angles (□) 90° and (○) 150°.

Analytically the calculated values for the hydrodynamic radius are presented in Table 3.4 that follows.

Table 3.4

Concentration in toluene	50wt%	88wt%	100wt%
R _H (nm)	43	35	27

Again we observe a decrease of the micelles size as the total polymer concentration increases assuming that at first there is solvent in the core that evaporates and the micelles become more compact. Also comparing the results of this linear copolymer with the respective I₂S#5 graft copolymer, we observe that again the sizes of the micelles that

we measure are relatively larger for the linear copolymer. This is in agreement with our results for the other pair of copolymers with $f_{PS} \sim 0.3$. Theoretical calculations that have been done, both for A-B diblock copolymer in B homopolymer, or for AB_2 graft copolymer in B homopolymer, forming spherical micelles, predict that the linear copolymer micelle consist of more chains resulting thus in larger sizes.⁽⁵⁾ If we use the molecular characteristics of the samples used in this work we find that the radius of the micelles formed by the linear copolymers should be 1.28 ($f_{PS} \cong 0.3$) up to 1.38 ($f_{PS} \cong 0.65$) times larger than the micelles formed by the graft copolymer. Our experimental results are in qualitative agreement with these theoretical predictions.

Concluding the results of this work on copolymer/homopolymer blends, the main aspects are the following: The sample containing the graft copolymer I₂S#5, which is the one with the highest composition in polystyrene showed micelle formation in all copolymer and total polymer concentrations investigated. In contrast with that, the mixture containing I₂S#1 graft copolymer that is poor in PS ($f_{PS}=0.09$) does not form micelles in any case. Finally, the mixture with 1wt% of the graft copolymer I₂S#3, which has an intermediate composition ($f_{PS}=0.32$), showed a concentration dependence of the micellization.

The respective linear diblock copolymer/homopolymer blends showed similar behavior to the graft ones. More precisely, the blend with the polyisoprene-polystyrene linear copolymer with $f_{PS} = 0.29$ that has similar composition with I₂S#3, indicated micelle formation above a certain total polymer concentration in toluene, which is very similar with the concentration that there is micelle formation at the I₂S#3/PI system. Moreover, the linear diblock copolymer with similar composition with I₂S#5 also showed micelle formation in the homopolymer matrix, in all copolymer and total polymer concentrations.

In general we observe that in the case of linear copolymers we find micelles with relatively bigger hydrodynamic radius a result that is in agreement with theoretical calculations for these systems.

B. Rheology

After the DLS measurements that have been performed for these samples, further investigation followed concerning their rheological behavior. For the purpose of this work two strain controlled Ares rheometers have been used, the one is equipped with parallel plate and Couette geometries and its temperature is bath controlled above 5°C; whereas the other has been used only in the parallel plate geometry for low temperatures (below 0°C) measurements under nitrogen.

In the parallel plate geometry the diameter of the plates was 25mm and the thickness of the sample was ~0.5-1 mm. The samples were measured in solutions in toluene as well as in the bulk state. For the solutions a solvent trap was used, in order to prevent evaporation of the solvent and therefore a change in the concentration during the experiment. All samples were prepared the same way as those for the DLS measurements; first the copolymer was dissolved in pure toluene and stirred for 24 hours. Then the PI was added and stirred again until a homogenous solution was obtained.

Both steady and dynamic measurements have been carried out. From the steady experiments the viscosity of the system was measured. In the dynamic measurements Dynamic Time Sweep tests were first performed to ensure that the sample is in equilibrium, which were followed by Dynamic Strain Sweep tests at a constant frequency to verify that the system is in the linear viscoelastic regime. The dynamic behavior of the sample has been studied with Dynamic Frequency Sweep in the linear viscoelastic regime.

3.6 Steady measurements

Figure 3.40 shows a steady rate sweep measurement for a PI 50wt% in toluene at $T = 293\text{K}$. The shear viscosity is defined as $\eta = \tau / \dot{\gamma}$ (eq. (2.22)), where the shear stress τ has come to a steady state. From this measurement the viscosity of PI 50wt% in toluene is calculated to be $\eta = 0.014\text{ Pa s}$. This value is almost 20times higher than the viscosity of pure toluene, $\eta_{\text{tol}} = 0.00059\text{ Pa s}$ and this makes the pure PI a quit viscous liquid.

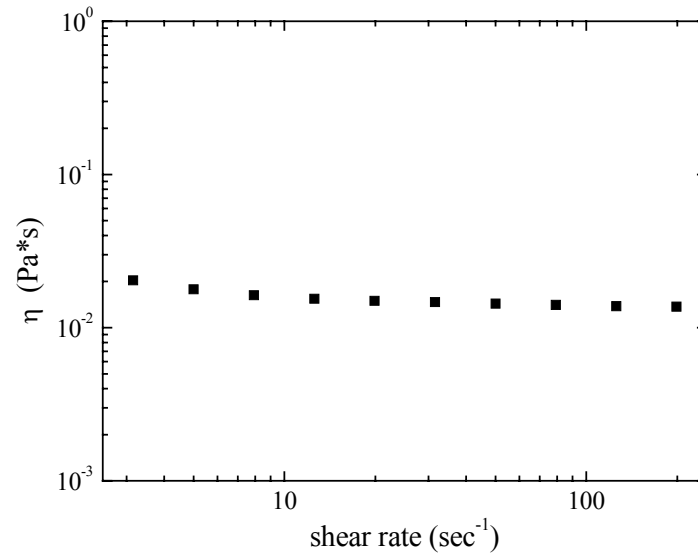


Figure 3.40 Viscosity of polyisoprene 50wt% in toluene at T=20 °C.

In order to investigate the dependence of the viscosity on the concentration, we performed several measurements in different polymer concentrations. In the following Figure 3.41 the results of these measurements are shown for polymer concentrations from 50wt % till bulk, at 20°C.

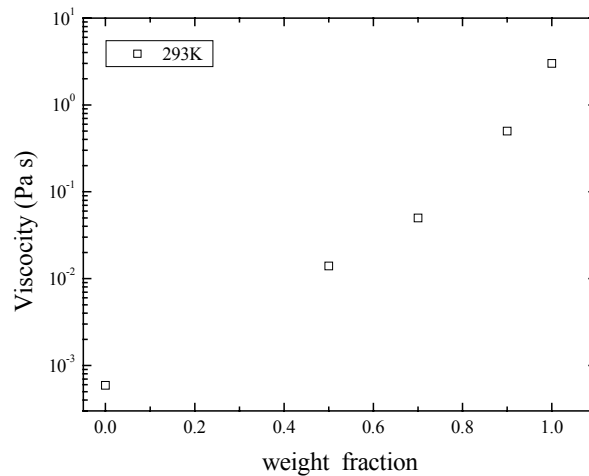


Figure 3.41 Concentration dependence of the viscosity of polyisoprene in the bulk state, at T=293K.

We observe that there is a strong dependence of the viscosity on the concentration. For the bulk state, the viscosity is equal to $\eta = 3 \text{ Pa s}$, almost two orders of magnitude higher than at concentration 50wt% in toluene. This change of the viscosity as a function of the concentration has been taken into account, in order to calculate the hydrodynamic radius R_H for DLS results (Chapter 3A).

Figure 3.42 shows the change of the viscosity as a function of the inverse temperature. The viscosity, as expected, decreases sharply as the temperature increases. It is known from the literature⁽⁶⁾ that viscosity has temperature dependence according to the Vogel Fulcher Tammann (VFT) equation:

$$\eta = \eta_0 e^{\frac{\beta}{T-T_0}} \quad (3.3)$$

where η_0 , β & T_0 are constants and T the temperature. For this case we have used $\eta_0 = 10^{-4} \text{ (Pa s)}$, $\beta = 1557\text{K}$ & $T_0 = 146\text{K}$ in order to fit our data.

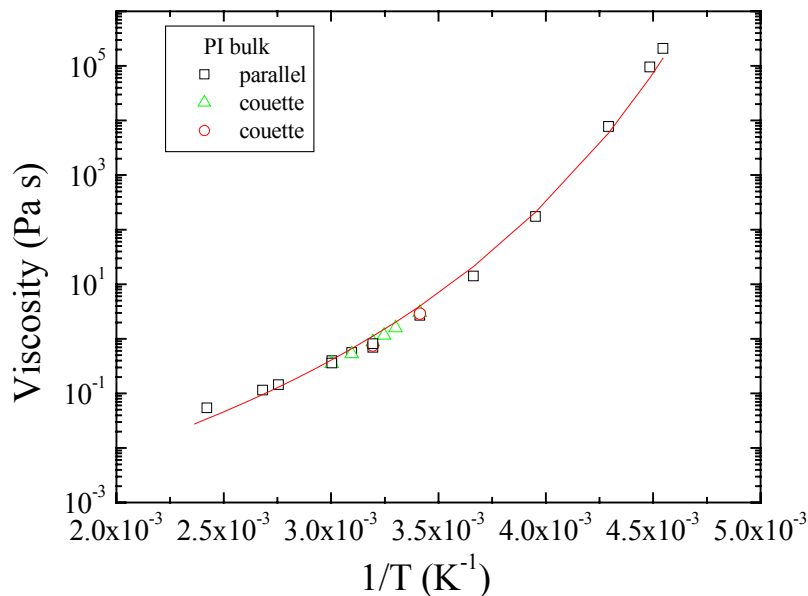


Figure 3.42 Viscosity of polyisoprene in temperatures from 213 to 413 K. Symbols: $\triangle \circ \square$ correspond to the parallel plate and couette geometry.

The parameters used for the above fit are very similar with those found in former work⁽⁶⁾ for PI of similar molecular weight. Namely, for polyisoprene of 4000 molecular weight, they had used $\beta = 1560\text{K}$ and $T_0 = 156\text{K}$. Notable is that all different geometries used, gave the same results.

Lastly, it should be mentioned that the temperature range for the viscosity measurements in the bulk was restrained by the fact that the glass transition temperature of PI is at $T_g = -65\text{ }^\circ\text{C}$, so all our measurements had to be performed well above the T_g .

3.7 Dynamic measurements

3.7.1 Polyisoprene

At this part of the work, first time and strain sweep experiments were performed in order to check the equilibrium state of the sample and to determine the regime that the sample exhibits a linear viscoelastic behavior.

Figure 3.43 shows a typical dynamic time sweep (dts) measurement. The sample investigated is PI homopolymer, in the bulk state at 233K. The measurement was performed with strain of $\gamma = 0.1\%$ and frequency $\omega = 10\text{Hz}$. It is clear that storage, G' , and the loss, G'' , moduli as well as the viscosity, η , are constant through the whole time range, suggesting that the system had reached the equilibrium state.

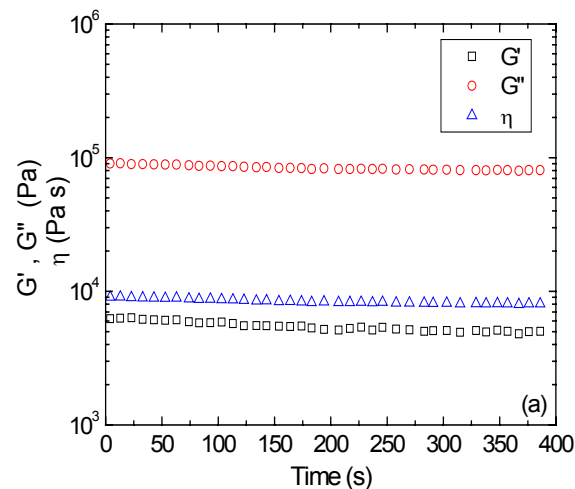


Figure 3.43 The time dependence of storage modulus (\square) G' , loss modulus (\circ) G'' and viscosity (\triangle) η , for PI homopolymer at 233K.

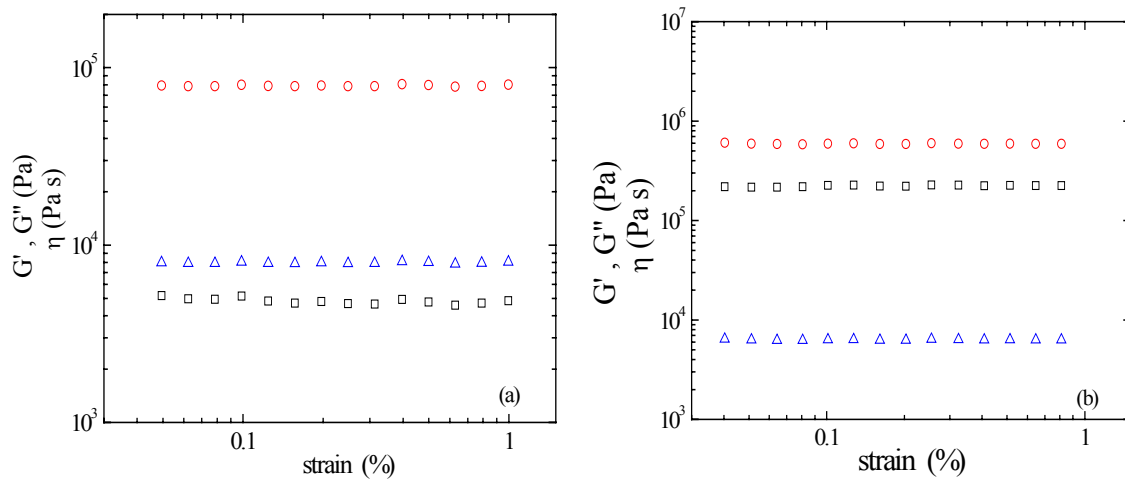


Figure 3.44 Storage (\square) G' , loss (\circ) G'' moduli and viscosity (\triangle) η , for PI homopolymer at 233K as a function of shear strain at (a): 10Hz (b): 100Hz.

Furthermore we perform dynamic strain sweep (dss) at a low (10Hz) and a high (100Hz) frequency, in order to ensure that the sample will be in the linear regime for all the frequencies that will be used later for the frequency sweep. Figures 3.44(a) and (b) show that G' , G'' and η are constant through the particular strain range, namely 0.03-1%, for both frequencies, indicating the linear viscoelastic regime for this sample.

The dynamic behavior of the samples has been studied extensively through dynamic mechanical spectroscopy that gives information about the structural rearrangements of the sample, with frequency sweep experiments in the linear viscoelastic regime. Typical results for the storage and loss moduli are shown in the Figure 3.45 for PI in the bulk state at the $T = 233\text{K}$.

The slopes of the storage G' and loss G'' moduli confirm that the sample is in the flow regime, since they follow the predicted scaling laws,⁽⁸⁾ that is:

$$\begin{aligned} G'' &\sim \omega \\ G' &\sim \omega^2 \end{aligned} \quad (3.4)$$

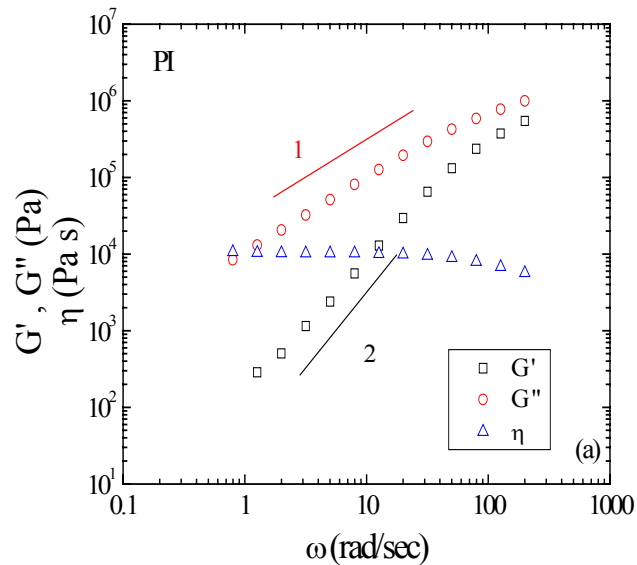


Figure 3.45 Storage modulus (\square) G' , loss modulus (\circ) G'' and viscosity (\triangle) η for PI at 233K with strain=0.1%.

From this measurement the viscosity of the sample can also be calculated at the low frequency limit:

$$\eta = \lim_{\omega \rightarrow 0} \frac{G''(\omega)}{\omega} \quad (3.5)$$

and it is found to be almost 10^4 Pa s, almost four orders of magnitude higher than at $T = 20^\circ\text{C}$, as calculated from the steady measurements.

3.7.2. I₂S#1 in PI

The rheological measurements were continued with the study of I₂S#1 block copolymer in PI in order to investigate the influence of the addition of the copolymer in the homopolymer matrix. In Figure 3.46 the dynamic frequency sweep of I₂S#1 at 1wt% in PI homopolymer is shown, at the bulk state and at temperature $T=313\text{K}$. This measurement, again, followed the dynamic strain and time sweep that always is performed for the reasons mentioned previously. The strain that was chosen in order the sample to be in the linear viscoelastic regime is 25%.

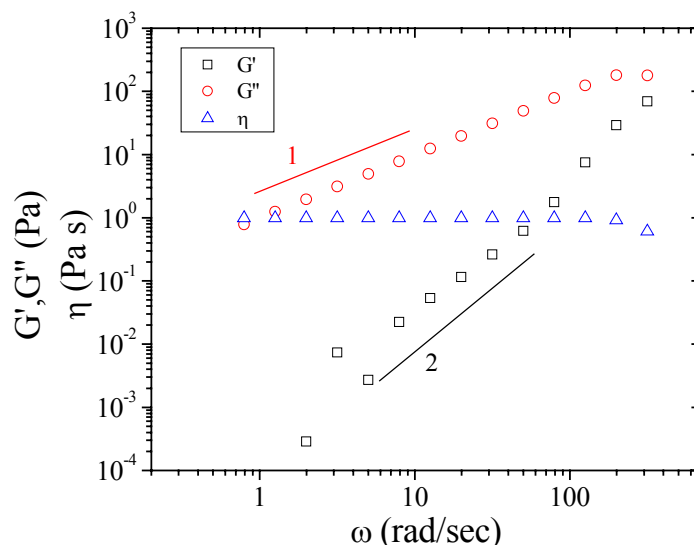


Figure 3.46 Dynamic frequency sweep of I₂S#1 1wt% in PI at T=313K. Storage modulus (\square) G' , loss modulus (\circ) G'' and viscosity (\triangle) η .

From this measurement, we can observe that the slope for the G'' is equal to 1 and for G' is 2. This indicates that again the sample is in the flow regime and this is confirmed from measurements in a wide range of temperatures from 293K until 343K. Additionally, Figure 3.46 shows the viscosity of this sample at 313K, $\eta=1\text{Pa s}$ and is similar with that of PI at the same temperature ($\eta=0.7\text{ Pa s}$).

This amount of copolymer in the sample doesn't seem to exhibit any specific change on the rheological behavior in comparison with that of pure PI. Furthermore, also the doubling on the amount of the copolymer in the homopolymer matrix does not show different results. Figure 3.47 shows the results of a dfs measurement for I₂S#1 2wt% in PI at 253K where the slopes are again those for the flow regime, since the loss and storage moduli are of the form $G'' \sim \omega$, $G' \sim \omega^2$. The strain in this case was 15%. The same results come out from measurements on temperatures from 213K until 293K.

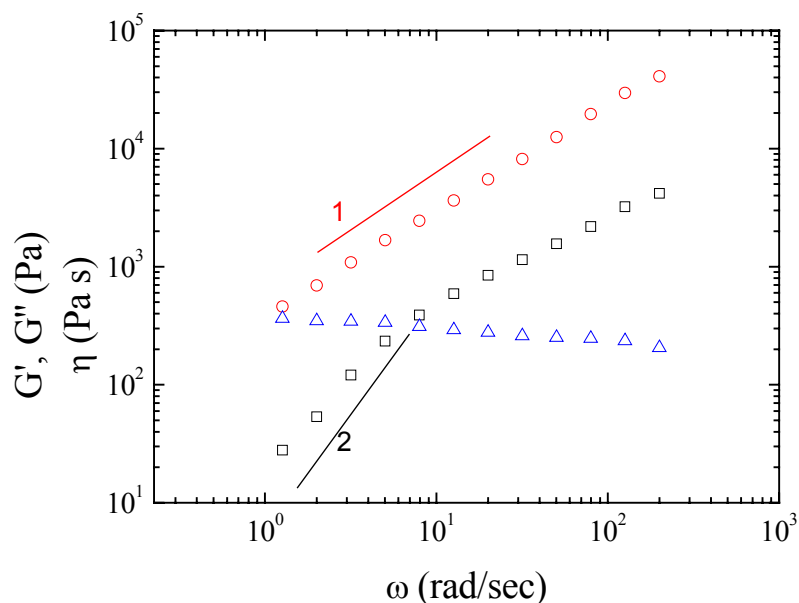


Figure 3.47 Dynamic frequency sweep of I₂S#1 2wt% in PI at T= 253K. Storage modulus (\square) G' , loss modulus (\circ) G'' and viscosity (\triangle) η are shown as a function of frequency.

3.7.3. I₂S#5 in PI

The results from the addition of I₂S#1 copolymer in polyisoprene led us to the investigation of samples that consists of PI with I₂S#5. This copolymer, as concluded from the DLS (section A), forms micelles in all examined concentrations. Steady shear measurements were first performed for the polymer that consists of 1wt % or 2% I₂S#5 copolymer. The results for the temperature dependence of their viscosity are shown in the Figure 3.48 that follows and they are compared to that of pure PI.

The predicted exponential dependence of the viscosity⁽⁶⁾ is observed also for these samples and the data can be fitted using the same parameters as for PI. From these results we can assume that there is no deference on the viscosity of PI with or without copolymer, since as we can conclude from Figure 3.48, they overlap. The values are determined strongly from PI independently if micelles are present or not. This behavior characterizes also the dynamics of these samples, as it will be shown below.

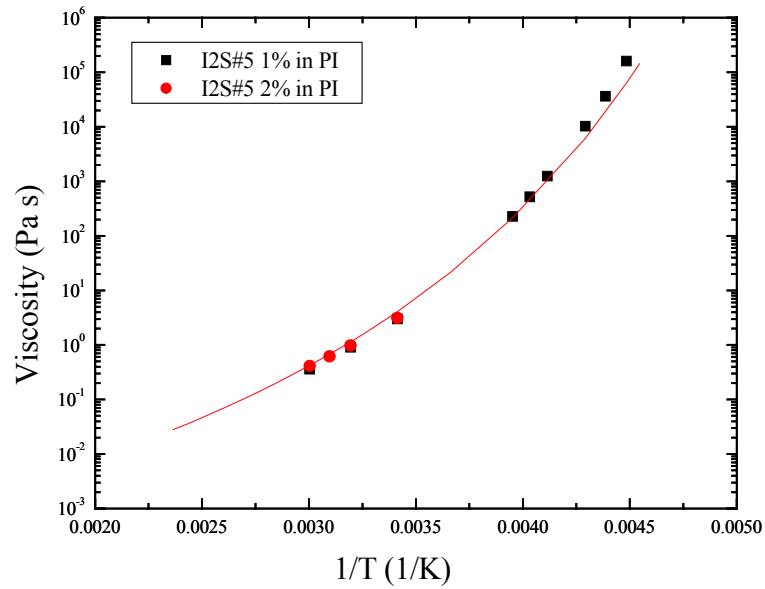


Figure 3.48 Viscosity of I₂S#5 1% and 2% in PI as a function of temperature. Red line is the VFT fit, used for PI results.

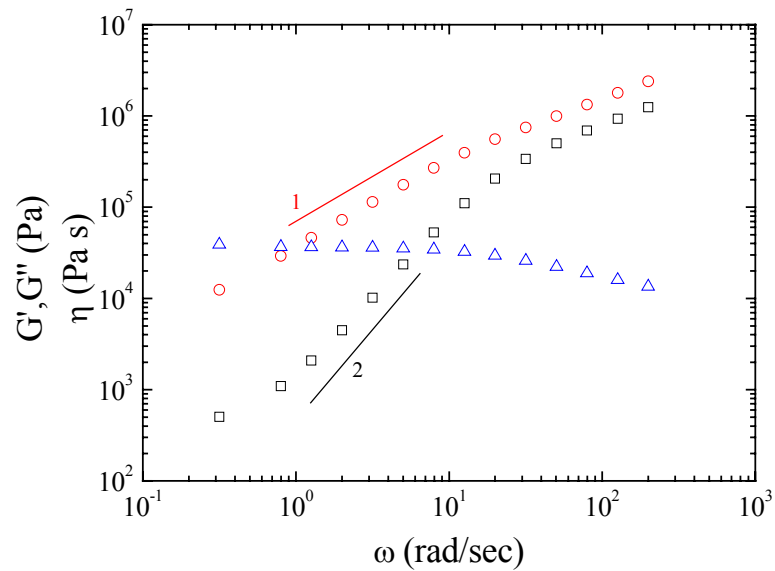


Figure 3.49 Storage modulus (\square) G' and loss modulus (\circ) G'' for I₂S#5 1% in PI at 228K strain 2%.

Figure 3.49 shows the results of the dynamic frequency sweep for I₂S#5 1wt% in PI at 228K. It is clear that the sample shows once more the flow regime without any specific difference in the shape of the storage, G' , and the loss, G'' , moduli curves, in comparison with the pure homopolymer at similar temperature (Figure 3.45). Consequently there is insensitivity of the rheological behavior of the polymer, not only to the addition of a copolymer in the homopolymer, but also to the presence of micelles. These assumptions had to be proved for as many different temperatures of the sample as possible in order to succeed completed results.

The investigation of this sample has been completed with experiments in different temperatures, extending the frequency region and covering the whole frequency spectrum. From the frequency sweep measurements for a wide range of temperatures (223K until 253K) we have managed to perform time temperature superposition (TTS) for 1wt% I₂S#5 copolymer that forms micelles in PI matrix, as it is shown in the Figure 3.50(a).

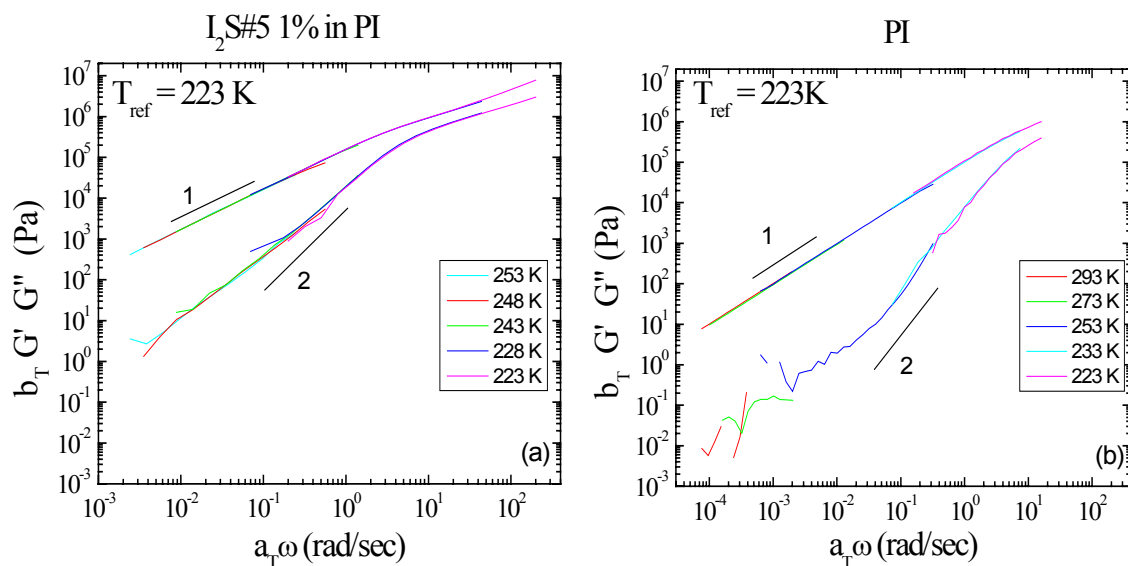


Figure 3.50 (a): Storage modulus, G' , and loss modulus, G'' , for I₂S#5 1% in PI in the bulk state, at reference temperature 223K. (b): Storage modulus, G' , and loss modulus, G'' , for PI in the bulk state.

Again in order to see the difference between PI with 1wt% I₂S#5 copolymer and pure PI, we have performed dynamic frequency sweep measurements in temperatures from 223K till 293K for the latter, as well. For this sample TTS worked also and the results are shown in the Figure 3.50(b). For the TTS the data were shifted along the frequency axis by a shift factor a_T to form collapsed curves, at reference temperature $T_{ref}= 223K$ and along the vertical axis using shift factor b_T that has the form:

$$b_T = \frac{\rho(T_{ref}) \cdot T_{ref}}{\rho \cdot T} \quad (3.7)$$

where ρ is the viscosity at temperature T .⁽⁸⁾

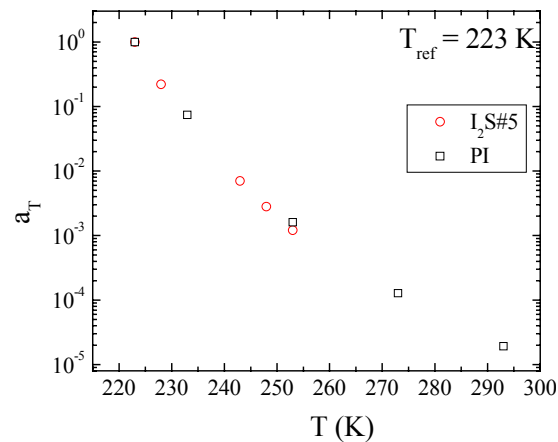


Figure 3.51 Shift factor a_T used in order to perform TTS for each sample, (\square) PI and (\circ) I₂S#5 1wt% in polyisoprene.

From the comparison of these plots, we conclude that at all temperatures investigated, I₂S#5 in PI does not differ from pure PI. We also observe that the shift factor a_T that we used for the TTS is similar for the two systems (Figure 3.51).⁽⁸⁾ Finally, we conclude that the presence of micelles does not affect the rheological behavior of the system. Former work⁽⁹⁾ that has been performed on the rheological response of linear diblock copolymers with similar molecular weight with the ones used

in the current work, showed that the increase of the copolymer concentration influenced the loss and storage moduli, which showed a plateau in the low frequency regime. This was happening, though for copolymer concentrations above 4wt%, whereas no effect was observed at copolymer concentrations below 2wt%. In our results, there is no indication of the existence of a plateau in the data as mentioned in previous works⁽⁹⁾ possible because we are in the dilute micelle regime and not close to their critical gel concentration (cgc) so we assume micelles are dilute and don't interact with each other.

References

- (1) Anastasiadis, S. H.; Chrissopoulou, K.; Fytas, G.; Fleischer, G.; Pispas, S.; Pitsikalis, M.; Mays, J. W.; Hadjichristidis, N. *Macromolecules* **1997**, *30*, 2445
- (2) Gercharz, B.; Meier, G.; Fischer, E.W. *J.Chem. Phys.* **1990**, *92*, 7110
- (3) Anastasiadis, S. H.; Fytas, G.; Vogt, S.; Fischer, E. W. *Europhys. Lett* **1993**, *26*, 619
- (4) Jian, T.; Anastasiadis, S. H.; Samenov, A. N.; Fytas, G.; Adaeli, K.; Kotaka, T. *Macromolecules* **1994**, *27*, 4762; Balsara, N.P.; Stepanek, P.; Lodge, T. P.; Tirell, M. *Macromolecules* **1991**, *24*, 6227
- (5) Retsos, H.; Anastasiadis, S. H.; Pispas, S.; Mays, J. W.; Hadjichristidis, N. *Macromolecules* **2004**, *37*, 524
- (6) Karatasos, K.; Anastasiadis, S. H.; Semenov, A. N.; Fytas, G.; Pitsikalis, M.; Hadjichristidis, N. *Macromolecules* **1994**, *27*, 3543
- (7) Larson, R. G. *The Structure and Dynamics of Complex Fluids*, Clarendon Press, Oxford, **1999**
- (8) Ferry, J. D. *Viscoelastic Properties of Polymers*, Wiley, J. and sons, **1980**
- (9) Watanabe, H.; Kotaka, T.; *Macromolecules* **1984**, *17*, 342

Chapter 4

Conclusions and Future Work

The architecture, composition and concentration effect on micellization in copolymer/homopolymer blends has been investigated in solutions in neutral good solvent toluene and in the bulk by DLS and Rheological measurements. Three (polyisoprene)₂(polystyrene), I₂S, graft copolymers with similar molecular weights and different polystyrene composition ($f_{PS} = 0.09, 0.32$ and 0.65) were utilized in the matrix of a low molecular weight polyisoprene.

A composition dependence of the micellization of graft copolymers has been observed. The sample containing the graft copolymer I₂S#5, which is the one with the highest polystyrene content, has been studied in three copolymer concentrations in polyisoprene (2, 1, 0.5wt%) and in a range of total polymer concentrations in toluene. In all concentrations micelle formation is observed with the size of the micelles being independent of the copolymer concentration (~22nm in the bulk). The size of the micelles, though, depends strongly on the concentration in the solution and the micelles become smaller as the amount of the solvent in the sample decreases. This is attributed to the presence of the solvent in the micelle's core as well as in the corona,

that is reduced with the evaporation of the solvent. This increase of the total polymer concentration leads to more compact micelles.

In contrast with the previous copolymer/homopolymer mixture, the one containing I₂S#1 graft copolymer which has a short polystyrene block ($f_{PS}=0.09$) does not form micelles in any copolymer (2, 1, 0.5wt%) or total polymer concentration, as indicated by the very low scattered intensity.

Finally, the mixture with 1wt% of the graft copolymer I₂S#3, which has an intermediate composition ($f_{PS}=0.32$), showed a concentration dependence of the micellization. For total polymer concentrations below 55wt% there are no micelles in the sample. At this concentration, and even more obvious above 60wt%, micelles are formed. These micelles have concentration dependent size that is reduced as the total polymer concentration increases.

Two linear polystyrene-*b*-polyisoprene diblock copolymers with similar weights and compositions with the graft ones were utilized in PI in order to examine the effect of the different architecture in the formation of micelles. The linear diblock copolymer/homopolymer blends showed similar behavior to the graft ones. More precisely, the blend with the polyisoprene-polystyrene linear copolymer with $f_{PS}=0.29$ that has similar composition with I₂S#3, indicated micelle formation above 54wt% total polymer concentration in toluene. For this sample, the size of the micelles decreases with the concentration, as well, and close to the bulk is ~39nm. Moreover, the linear diblock copolymer with similar composition with I₂S#5 showed also micelle formation in the homopolymer matrix, in all copolymer (2, 0.5wt%) and total polymer concentrations. The size of these micelles in the bulk was ~27nm.

Although, the concentrations and compositions that there are micelles in the samples are similar between the linear and graft copolymers, the micelles formed by the linear copolymers are relatively larger than the ones formed by graft copolymers, in agreement with theoretical predictions.

All these similarities and differences among the various systems were observed from the DLS measurements. In contrast, the presence of the micelles in the sample did not indicate any effect on the rheological results. Both the viscosities and the storage and loss moduli were found to behave similarly, independently either of

the presence of the copolymer chains or of the micelles probably due to the low copolymer concentrations used, which is in the dilute micelle regime.

A continuation of the current work is in progress. The same series of graft copolymers are being investigated through SAXS measurements in more copolymer concentrations in order to evaluate the critical micelle concentration, cmc, the aggregation number of these micelles or the temperature dependence of micellization. At the same time, the effect of the different architecture on the micelle formation is examined by utilizing graft copolymers with two polystyrene and one polyisoprene blocks and systems with star-like architecture.